Ca' Foscari
University
of Venice

Master Degree programme

in
"Environmental Sciences"
"D.M. 270/2004"

Final Thesis

Ocean Dynamics in the Subpolar North Atlantic: spatial and temporal variability of the Subpolar Gyre in a high resolution ocean – atmosphere regionally coupled model

Supervisor
Ch. Prof. Davide Zanchettin

Assistant supervisor
Ch. Prof. Angelo Rubino

Graduand
Carlotta Dentico
Matriculation Number 843484

Academic Year
2018 / 2019

TABLE OF CONTENTS

GLOSSARY

SPG					Subpolar Gyre
AMOC					Atlantic Meridional Overturning Circulation
NAC					North Atlantic Current
IC					Irminger Current
EGC					East Greenland Current
WGC					West Greenland Current
LC					Labrador Current
LSW					Labrador Sea Water
GSR					Greenland-Scotland Ridge
NADW					North Atlantic Deep Water
NAO					North Atlantic Oscillation
ESMs					Earth System Models
ROM					REMO – OASIS – MPIOM
REMO					REgional atmosphere MOdel
MPIOM					Max Plank Institute Ocean Model
HAMOCC					HAMburg Ocean Carbon Cycle
HD					Hydrological Discharge
GCMs					Global Circulation Models
AOGCM					Atmosphere Ocean General Circulation Model
CGCM					Coupled General Circulation Model
RCMs					Regional Climate Models
RAOCMs					Regional Atmosphere Ocean Climate Models
SST					Sea Surface Temperature
SSS					Sea Surface Salinity
TFWF					Total Fresh water Fluxes
DWBC					Deep Western Boundary Current

SUMMARY

The SPG is a critical component of the Earth's climatic system, as it modulates the exchange of heat and salt between the North Atlantic and Arctic Ocean, and it interacts with large scale oceanic features like the Atlantic Meridional Overturning Circulation and the Global Thermohaline Circulation.

Currently, the SPG variability is thought to be largely controlled by an east-west seawater density gradient in the SPG region that is determined by the contrast between hot and salty water masses from mid-latitude Atlantic Ocean, mainly transported by the Gulf Current, and fresh and cold water masses from the Arctic Ocean.

I investigate ocean dynamics in the North Atlantic Subpolar Gyre (SPG), using a state-of-the-art global ocean – regional atmosphere coupled model. The goal of this research is to determine whether this mechanism is active in this state-of-the-art Earth system coupled model. To this purpose, I focus on interannual and decadal variability of the SPG, identified by variations in the mass barotropic streamfunction. I used an ensemble of three simulations with ocean-atmosphere coupling activated in the Tropical Atlantic that have different atmospheric resolution. Secondly, I compared them to an additional simulation where the ocean-atmosphere coupling is activated in the SPG/Arctic instead of in the Tropical Atlantic to show different contributions to SPG dynamics. Specifically, the effect of heat and salt from the Tropical Atlantic and fresh water fluxes and sea ice expert from the Arctic. At the end I also evaluate the linkages between SPG and the Atlantic Meridional Overturning Circulation (AMOC), especially their relationship with meridional ocean transport of heat and mass.

The investigation makes use of statistical methods to identify lead-lag relationships between the SPG variability and selected driving variables as triggers of the described variability (sea surface temperature, sea surface salinity, density, fresh water fluxes and anomalies of sea ice fraction in Denmark Strait) and heat and mass transport in the AMOC. This includes also time series analysis, cross-correlation and linear regression analysis and wavelet analysis.

A first key aspect of the research is the identification of patterns that can explain the described variability in the three simulations i.e. whether this variability is due to internal variability or to external forces showing temporally varying spatial patterns in the relationship between SPG and the driving variables to unveil sources and pathways of SPG variability. Secondly to show the connection

between SPG variability and large scale features like the AMOC and the possible consequences which changes can have in the European climate, Sea Ice dynamics and global circulations.

THESIS STRUCTURE

This Thesis is structured in three main sections: Section A provides an overall picture of the theoretical background; Section B describes the methodological development of this thesis; Section C presents the results associated with the main scientific questions.

More specifically:

Section A, after a short introduction on the main features that characterized the Subpolar gyre (SPG) basin, presents the state-of-the-art of numerical models in climate science. It further provides a brief discussion and comparison between classical Earth System Model and the state-of-the-art model used in the present Thesis.

Section B describes the methodological approach used in order to assess the SPG variability on interannual and decadal time scales. Moreover, the description of the four transient simulations setup, the description of the driving variables so far associated with SPG variability and the statistical analyses that have been performed.

Section C reports and critically analyses the results of the nature of the simulated SPG variability, together with the description of its relationship with the driving variables and elucidating the differences among the simulations.

Section D provides Discussion and Conclusions of the main findings obtained during the analyses, highlighting its main strengths and weaknesses as well as some recommendations for its future outlook of the present study.

INTRODUCTION

The subpolar gyre (SPG) is a dominant large-scale feature of the upper circulation of the Northwest Atlantic Ocean (Higginson *et al.*, 2011) and it represents a critical component of the Earth's climatic system (Rhein *et al.*, 2011). It is characterized by a cyclonic circulation pattern extending between 45° N to 65° N (Rhein *et al.*, 2011) and 60° W and 20° W. It is composed by a complex system of currents that modulate – and are, in turn, influenced by – the exchange of heat and salt between Atlantic and the Arctic Ocean. SPG dynamics, contribute, for example, to shape the European temperate climate (Marzocchi *et al.*, 2014) and the distribution of sea ice in the Arctic region (e.g., Yoshimori *et al.*, 2010; Jungclaus *et al.*, 2014). SPG variations, moreover, are intertwined with changes in the intensity and strength of the Atlantic Overturning Meridional Circulation (AMOC) (e.g., Hátún *et al.*, 2005; Moreno-Chamarro *et al.*, 2015) which contributes to explain the interdecadal and centennial time scales that dominate SPG variability and its climatic repercussions.

The SPG circulation, a simplified representation of which is shown in Figure 1, is composed by different currents that contributes to produce buoyancy contrasts between the basin center and its boundaries (e.g. Langehaug *et al.*, 2012).

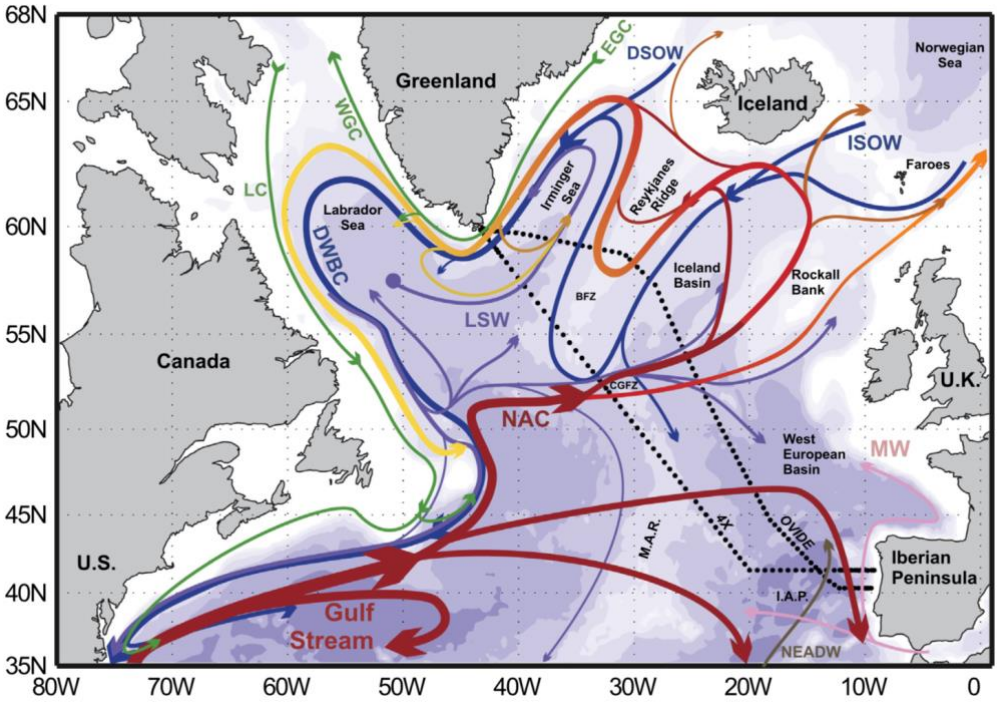

*Figure **1** Schematic representation of the North Atlantic circulation scheme, the major topographical features of the Subpolar North Atlantic, as well as the main water masses are also shown: East Greenland Current (EGC), West Greenland Current (WGC), Labrador Current (LC), Deep Western Boundary Current (DWBC), North Atlantic Current (NAC), Denmark Strait Overflow Water (DSOW), Iceland–Scotland Overflow Water (ISOW), Labrador Sea Water (LSW), Mediterranean Water (MW), North East Atlantic Deep Water (NEADW), Charlie–Gibbs Fracture Zone (CGFZ), Bight Fracture Zone (BFZ), Mid-Atlantic Ridge (M.A.R.) and Iberian Abyssal Plain (I.A.P.) from Ibáñez et al., 2015.*

On the one side, hot and salty water masses that flow poleward from tropical and subtropical regions of the Atlantic Ocean towards the eastern part of the SPG basin. These waters contribute to the warm and salty upper branch of the AMOC and are transported to and within the SPG basin trough the Gulf Stream, the North Atlantic Current (NAC) and the Irminger Current (IC). On the other side, cold and fresh waters flow equatorward from the Arctic as floating sea ice and low-salinity water from sea-ice melting and from the runoff from the North America and Greenland ice cap (e.g. Dickson *et al.*, 2007). This water masses flow along the eastern and western shelves of Greenland trough the West Greenland Current (WGC), which successively flows into the Labrador Current (LC), and by the East Greenland Current (EGC). These currents are essential for the transport of high latitudes water into the subtropical and tropical ocean basins (Higginson *et al.*, 2011). A great part of the exchange between the cold and deep Nordic Seas and the Arctic Ocean waters and the rest of the world ocean water masses, happen across Greenland, Iceland and the Faroe Island where there is a ridge system, the Greenland-Scotland Ridge (GSR) (e.g. Marzocchi *et al.*, 2014; Bacon, 2002). The sills in the GSR, dams up the deep waters from the Arctic and Nordic Seas thus largely controlling the density difference between such basins and the North Atlantic. Relatively cold and fresher Nordic seas water pass over the top of the sill and flow downstream even at depth 1000-2400 m, especially in winter times, generating the so called GSR dense overflow (Bacon, 2002).

The climatic relevance of the SPG is not limited to its modulation of mass and heat transport by horizontal ocean currents: the SPG basin is also a crucial ocean region for deep and intermediate waters formation (Katsman *et al.*, 2004). One of the two more active regions for the deep water formation, is the Irminger Sea where the warm branches of the NAC and the IC release heat to the atmosphere causing a buoyancy loss and the consequent formation of intermediate and deep waters. In the Labrador Sea, the energy is exchanged between the atmosphere and the ocean surface (Rhein *et al.*, 2011) resulting in the generation of an important intermediate water mass, the Labrador Sea Water (LSW) that is one of the main element of the AMOC. Deep water formation and overflows in the SPG region contribute to generate a dense and cold deep water that flows southward, known as the North Atlantic Deep Water (NADW) (e.g. Rhein *et al.*, 2011) which constitutes the deep branch of the North Atlantic thermohaline circulation (e.g. Dickson and Brown, 1994) . This deep return current is a key process for the transport of heat, freshwater, carbon dioxide, in the global world ocean-atmosphere system (e.g. Haine *et al.*, 2008). Thus, variations in the strength and shape of the SPG can lead to major changes in the intensity of the AMOC and in the global thermohaline circulation (e.g., Hátún *et al.*, 2005; Moreno-Chamarro *et al.*, 2015).

SPG variability can be induced by changes in wind forcing and surface buoyancy fluxes: for instance, a known factor of such variability are the changes in the phase of the North Atlantic Oscillation (NAO), the dominant mode of large-scale atmospheric variability in the Northern Hemisphere (e.g., Eden and Willebrand, 2001; Deshayes and Frankignoul, 2008). SPG variability can also be induced by internal ocean dynamics, particularly related to horizontal gradients in the upper-ocean density between the gyre's center and its boundaries (Born and Stoker, 2014; Moreno-Chamarro *et al.*, 2016). Such gradients are particularly sensitive to LSW characteristics, where anomalously cold LSW, at the core of the SPG center, strength the zonal gradient of upper-ocean densities and force a spin-up of the gyre circulation.

Currently, there are only short and sparse instrumental oceanic observational records in the SPG region and estimates of the mean circulation based on such limited sampling could be seasonally biased and significantly omitting the low-frequency variability (Higginson *et al.*, 2011). Recognizing the gap of systematic observations of the SPG, an international program designed to provide a continuous record of the full-water column, trans-basin fluxes of heat, mass and freshwater in the subpolar North Atlantic has just started (https://ww.o-snap.org/). Therefore, characterization and understanding of SPG variability still largely relies on the use of numerical models. They are subject to careful evaluation and regarded as useful tools to investigate the mechanism of the complex systems in climate and environmental sciences (e.g. Flato *et al.*, 2011).

Much effort in recent decades has been devoted by the climate research community to develop efficient Earth System Models (ESMs) that include coupled representations of ocean and atmospheric physics, land surface processes including vegetation and land use, biogeochemistry, atmospheric chemistry, and the hydrological cycle (Taylor *et al.*, 2012). ESMs are typically used to simulate the longer-term evolution of the Earth's climate on decadal and longer time scales, for instance to explore the range of future climate warming under scenario of increased anthropogenic greenhouse gas emissions, but can also be used to make short and medium-range weather forecasts and seasonal predictions (realistically, they are not used since some internal configuration of such ESMs can't be used for weather forecast that required e.g. many repetition and very high resolutions of the simulations). Still, the need of ESMs to simulate the whole global climate poses a computational limitation on the amount of spatial details that current ESM simulations can provide: the horizontal spatial resolution most often remains above hundreds of kilometers in a global grid. Therefore, ESMs, have difficulties in accurately simulating weather and climate on regional and local scales and sometimes are affected by substantial systematic errors in the mean, seasonality and interannual variability over many areas of the globe compared to observations (e.g. Zanchettin *et al.*, 2017).

Several approaches have been developed to surpass such limitation, the most known being nested regional climate models that resolve a limited area of interest with high resolution and are forced at their lateral boundaries by the low-resolution output of a preexisting global ESM simulation. In this one-way downscaling, the regional climate model acts only as a physically-based nonlinear interpolator of the ESM, in the sense that the variability it generates is not allowed to affect the global climate evolution, hence the trajectories in both the regional and the global model do not diverge.

The novel downscaling approach by Sein *et al.*, (2015) allows to account for two-way interactions between dynamics of the global ocean and small-scale regional atmospheric dynamics. The resulting climate model consists of a global ocean-sea ice-marine biogeochemistry model with a curvilinear grid, which allows to obtain regionally a high horizontal resolution, coupled with an atmospheric regional model and a global terrestrial hydrology model. Outside the domain of the regional atmospheric model, the ocean model is forced by a wind stress and turbulent surface fluxes by reanalysis data (or any data from an ESM scenario simulation). Therefore, the ocean and the atmosphere interact freely within the region where the coupling is active, and the effects of such interaction reverberate on the circulation of the world ocean. The whole model is known with the acronym ROM (REMO – OASIS – MPIOM). It comprises the Regional atmosphere Model (REMO), the Max Planck Institute Ocean Model (MPIOM), the Hamburg Ocean Carbon Cycle (HAMOCC) model, and the Hydrological Discharge (HD) model, which are coupled via the OASIS coupler.

The present study aims to investigate temporal and spatial variability of the SPG strength in relation with selected driving variables using a novel approach of a classical coupled global ocean – regional atmosphere model.

Here, I used an ensemble of four ROM simulations with ocean-atmosphere coupling active in the Tropical Atlantic and in the SPG/Arctic region to investigate inter-annual to decadal changes in SPG intensity. The simulations use different resolutions of REMO and cover a period 32 years from January 1980 to December 2012 for three out of four simulations, and a period of 85 years from January 1920 to December 2005 for the last simulation. This study concentrates on the comparative temporal and spatial analysis of the output of these simulations to highlight the spatial and temporal SPG variability in relation with selected driving processes. In the interpretation of the ensemble results, the occurrence of differences among the simulations in the SPG evolution is associated with internal climate variability (the “random” variability that arises spontaneously in each simulation), whereas consistent behavior reveals the predominance of the effects of external forcing. Lead-lag correlation and linear regression analysis, and wavelet analysis will be used to investigate the mechanism of the simulated SPG variability, in particular aiming at identifying robust precursor of SPG variations. These

analyses will also reveal whether the dominant SPG mechanism in the different simulations are the same notwithstanding differences in the emerging SPG behaviors.

The main objective of the research is to evaluate if and how SPG mechanism is active in this state-of-the-art model and which are the relation and response to selected driving processes and variables, and, ultimately, with a large-scale oceanic feature like the AMOC. SPG variability is mainly related to surface buoyancy fluxes and by internal ocean dynamics related to horizontal gradients in the upper-ocean density, particularly sensitive in LSW mainly associated with changes in cold and fresh water export. For this reason, the selected driving variables used to describe the response and relation with SPG variability are the Sea Surface Temperature, Sea Surface Salinity, Density, Total Fresh Water Fluxes throughout the SPG basin and Sea Ice Fraction within the Denmark Strait. To do that, I first compare the results from three simulations that are initialized in the same period of time (32 years) with the coupling activated in the Tropical Atlantic with different resolutions of REMO. This is important when evaluating if SPG changes in intensity is due to internal variability of the systems, i.e. how the simulations are initialized or if its due to the effect of some external forces. I thus aim to answer the following research questions: (1) What is the nature (internally generated vs externally forced) of the simulated SPG variability on interannual to decadal time scales?, (2) Does a robust mechanism driving SPG variability exist, and which are its precursors? (3) Which are the main differences between the differently gridded simulations?, (4) Which is the evolution of SPG in relation to heat transport, fresh water fluxes and ice export?. Answer to these scientific questions will be further supported by inclusion of an additional ROM simulation where the ocean-atmosphere coupling is activated in the SPG/Artic region instead of in the Tropical Atlantic. This allows for a separation of the different contributions to SPG dynamics: heat and salt, that are transported to the SPG basin from the tropical Atlantic Ocean (forced externally, hence consistent among the first three ensemble simulations), and the fresh water fluxes and sea ice export from the Arctic (forced internally in the additional simulation). Finally, I will analyze the linkages between SPG and the AMOC especially concerning their relationship with meridional oceanic transport of heat and mass. The last research question I aim to answer is: (5) Which are the interactions between the AMOC, heat meridional heat transport and SPG strength?.

The thesis is organized as follows. First Section A provides a short discussion of the use of numerical models in climate science providing a brief comparative discussion between classical Earth System Models and ROM. Section B describes the ROM simulations and the list of the selected geophysical variables. The employed statistical methods including time series analysis, cross-correlation and

linear regression analysis and wavelet analysis can also be found in section B. Results are described in Section C. Discussion and Conclusion, including thesis outlooks, are given in Section D.

SECTION A: THEORETICAL BACKGROUND

1- The use of numerical models in climate science

1.1- State-of-the-art numerical models[1]

A climate model is a mathematical representation of the climate system based on physical, biological and chemical principles. These laws are approximated as complex equations numerically solved producing solutions that are discrete in space and time. The input of numerical models can be either observations or outputs of other model studies. Observations are essential, especially during the development phase of the model providing information on the properties of the studied system and to test the validity of the model. The results of a climate model are usually averaging over regions (can be globally or zonally averaged values or based on numerical grid) whose size depends on the model resolution, and are comprises in a specific time interval (from minutes to several years, depending on the process studied). Observations and the other model inputs are separated in *boundary conditions* (fixed variables) that remains constant during the entire course of the simulation but can also evolve interactively especially (e.g. in studying climate variations on longer time scale) and in *external forcing* that drives the changes in the event under study, being in many cases a key state variable of the model. The decision process of the variables that must be included in a model is essential during the model designing phase. Usually, in climate studies, the physical behavior of the atmosphere, the ocean and the sea ice must be included. The terrestrial and marine carbon cycle, the dynamics of the vegetation and the ice sheet components are now more included in climate models, an addition that has yield to the so-called Earth System Models (ESMs).

Currently, ESMs are considered the most comprehensive tools available for simulating past and future response of climate systems to external forcing and are the current state-of-the-art models most widely used (Flato et al., 2013). Scientists cannot always perform controlled experiments on large – scale systems (Griffies, 2003), but they use "virtual systems", thus one of the main advantages in the use of numerical models in climate science, lie in improving scientists' knowledges about the climate characteristics and to understand the cause of the climate variations in time. These advantages go with simplifications of processes, usually established by the objective of the study, since spatial and temporal scale are very. Simplifications depend also on technical issues since even in the most powerful computers some models can't be daily used for very long periods (few centuries

[1] Most of the information provided in this chapter are taken from Goosse *et al.,* 2010

to millennia) or when a large number of experiments are needed. The "ideal" model should be designed to include only the most important properties to deep understand the characteristics and the complex interactions between the multitude of components that characterized climatic systems. There is no perfect model suitable for all purposes and this is why a large range of different climate models exists. In general, combining the results from various types of models is often the best way to gain a deep understanding of the dominant processes in action.

Oceans are characterized by complex dynamics and most of the time, oceanographers are data poor since in situ data collection has becoming quite expensive. Remote sensing is also a valuable and wide used tool but, in some cases, it lacks capturing deep features or small-scales processes especially within the sea-atmosphere interactions. The use of numerical models applied in oceanographic studies has gained more and more attention in the last decades (Kantha and Clayson, 2000). Important progresses have been made in the resolution of the numerical simulations in the North Atlantic Ocean that has led to a simplification in the characterization of the geometry and bathymetry and in the development of fine-resolution simulations able to incorporate realistic coastal definition and bottom topography (e.g. Smith *et al.*, 2000). Accordingly, the SPG variability has becoming a very challenging study area for ocean modelers (Teguier *et al.*, 2005), since the complex ocean dynamics that characterize this region. Fully coupled climate models are considered a valuable tool for investigating the mechanisms controlling SPG variability on decadal to multidecadal time scales (e.g. Delworth and Mann 2000).

1.2- Classical Earth System Models (ESMs) and ROM: Comparative discussion[2]

An ESM can be simply defined as a synthesis of the interactions between the climate system and terrestrial and oceanic ecosystems that describe exchanges of energy, the chemical reactions, and all the processes and impacts produced on the physical climate (Flato, 2011). In last decades, a lot of work has been done to develop more accurate and detailed ESMs that can better described the interactions between atmosphere, ocean, land, ice and biosphere (Taylor *et al.*, 2012). ESMs can be a very effective tools to simulate the present state of the Earth's climate but also to simulate the evolution of the climate on decadal and longer time scales to produce short and medium-range weather forecast and seasonal predictions (Sein *et al.*, 2015).

[2] The model description and its main advantages are taken from Sein *et al.,* 2015

There are some limitations in the use of ESMs. They make difficult, for example, to simulate and represent important natural processes that operate on very small scales (Flato, 2011) and to simulate climate on regional and local scales (Sein *et al.*, 2015). Regional atmosphere – ocean climate model (RAOCMs) are able to achieve higher resolution and detailed parameterization, better representing complex morphological feature (like land-sea and atmosphere-sea interactions) and small-scale processes. ROM belongs to this category of models and, compared to others ROACM, can simulate regional climate from years to decades. This novel state-of-the-art model is a valuable tool to downscale climate simulations and to investigate the interactions especially between the North Atlantic and Arctic Ocean, in which SPG is comprised, but generally all the impacts of ocean-atmosphere interaction processes on the regional climate. ROM is composed by a regional atmospheric model (REMO) that is coupled with a global ocean-sea ice-marine biogeochemistry (MPIOM – HAMOCC) model with regionally high horizontal and global terrestrial hydrology model (HD). The technique of coupling divides global ocean model setup into two different subdomains: coupled, where the ocean and the atmosphere are interacting, and uncoupled, where the ocean model is driven by prescribed atmospheric forcing and runs in a so-called "*stand-alone mode*". The ROM coupled system has been seen to improve the representation of key climate variables on the regional scale especially in the ocean model, by including physical processes non-accounted in classical RAOCMs. This allowed, for example a more realistic representation of the Gulf Stream separation that, for instance, increases the tropical water inflow into the SPG basin that enhance deep water formation. ROM can be tested to show whether and how the SPG is active in this state-of-the-art model, since model studies in the north Atlantic Subpolar basin have been mostly restricted to hindcast simulations with ocean general circulation models (OGCMs) forced with atmospheric reanalysis fields (e.g. Hátún *et al.,* 2005; Böning *et al.*, 2006).

The model still has some disadvantages, for instance the limitation of the vertical resolution, i.e. the upper ocean model layer has to be thick enough to handle the ocean tides and underwater part of the sea ice. Another disadvantages regards the bias and internal variability generated from the global domain that can influence the result in the coupled domain and indeed the MPIOM component in ROM requires refinement of the computational grid in the coupled domain (even though, this does not mean that the ocean resolution outside the coupled area is neglected but the contrary it should be fine enough to reproduce general features of the global ocean circulation). Therefore, there is still potential for improvement.

1.3 – ROM Characteristics[3]

The ocean model MPIOM is a free surface, primitive equations ocean model, that uses the Boussinesq and incompressibility approximations. The model is formulated on an orthogonal curvilinear Arakawa C-grid (Arakawa and Lamb, 1977) with z-level vertical discretization. The curvilinear grid allows for the placement of the poles over land, thus removing the numerical singularity associated with convergence of meridians at the geographical North Pole, providing a high resolution in these regions. The model embedded sea ice dynamics and thermodynamics like sea ice thickness and fractional coverage that are calculated on the viscous-plastic rheology model based on Hibler, 1979. Sea ice thickness dynamics are related to a balance of radiative, turbulent and oceanic fluxes, while the fractional sea ice coverage is within grid cells calculated according Stössel, 1992. Subgrid-scale processes like slope convection and flows water masses for example over sills and off shelves have been differently parameterized. The dynamics and discretization in time and space of the model REMO is based on the Europa-Model of the German Weather systems (see Majewsky, 1991). REMO's prognostic variables are the surface pressure, horizontal wind component, temperature, water vapor, liquid water and cloud ice. REMO uses a rotated grid system, with the equator of the rotated system in the middle of the model domain, in order to avoid largely differences in the extension of the grid cells near the poles. The Hamburg Ocean Carbon Cycle model HAMOCC (Maier-Reimer, 1993; Maier-Reimer *et al.*, 2005) includes the relevant carbon stocks of the atmosphere, the ocean, and the sediments and simulates the exchange between them, while the Hydrological Discharge (HD) model (Hagemann and Dümenil, 1998; Hagemann and Dümenil Gates, 2001) simulates globally the lateral freshwater fluxes at the land surface.

The MPIOM and REMP models are coupled with the OASIS coupler developed by CERFACS (Valcke *et al.*, 2013). As the regional model (REMO) covers only a part of the global ocean, MPIOM needs to be run in both coupled (the branch REMO-OASIS-MPIOM, Figure 2) and stand-alone (the branch External Forcing-Bulk Formulae-MPIOM, Figure 2) modes simultaneously. The ocean model running in the coupled subdomain receives the heat, freshwater, and momentum fluxes calculated in REMO at specified frequency (coupling time step) and passes the sea surface conditions to the atmospheric model. In the uncoupled sub-domain, the ocean model calculates heat, freshwater, and momentum fluxes from the global, predefined atmospheric fields (e.g., from reanalysis data) using specific bulk formulas at a specified frequency (forcing time step). REMO obtains the lower boundary conditions

[3] the information about ROM characteristics are taken from Sein *et al.,* 2015

over the sea and sea ice surfaces from MPIOM through the OASIS coupler every coupled time step. Simultaneously, it provides the atmospheric momentum, heat and water fluxes to the ocean model. Thus, the OASIS coupler ‘‘sees’’ both models on the same REMO computational grid.

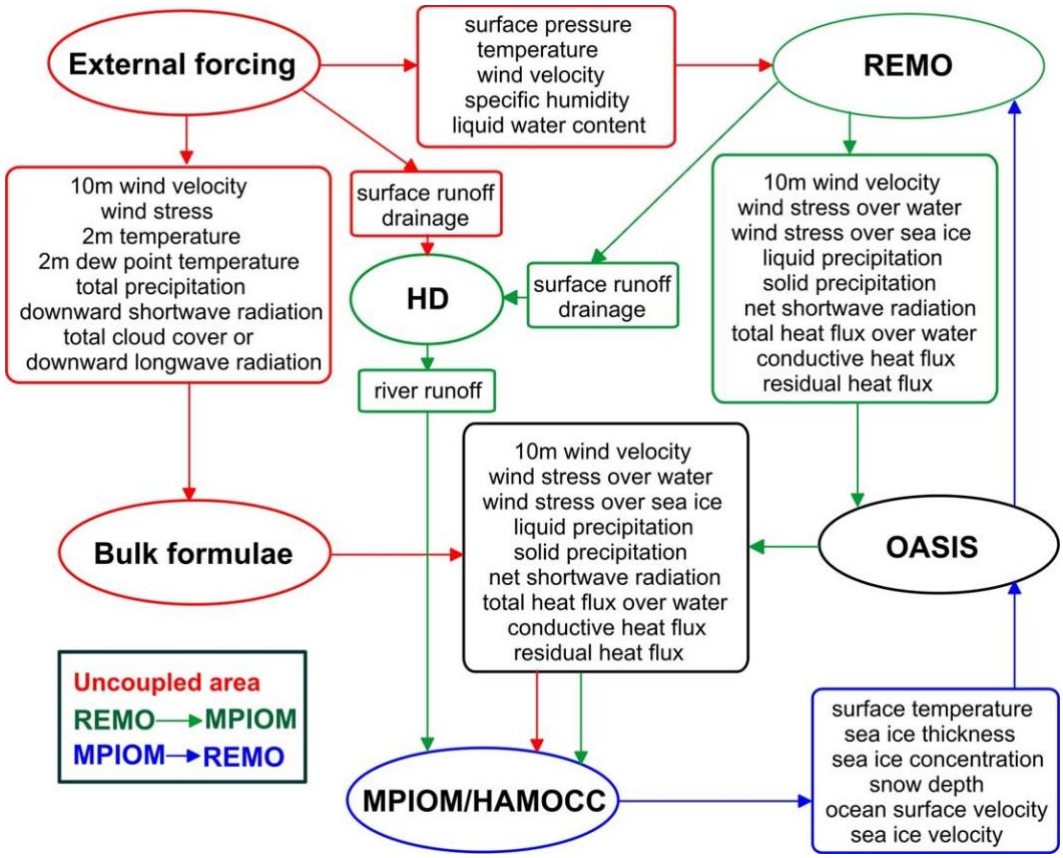

*Figure **2** Coupling scheme. Red color denotes the prescribed forcing used as lateral boundary conditions for REMO and as surface forcing for MPIOM in the uncoupled area. The workflow of heat, momentum, and mass fluxes from the atmosphere (REMO) to the ocean (MPIOM) from Sein et al., 2015.*

SECTION B: DATA AND METHODS

2.1 – ROM simulations setup

I evaluate the interannual to decadal variability of the SPG using four transient simulations from the state-of-the-art model ROM. The important characteristics and differences among the simulations are shown in Table 1. The *NAS, NAT* and *NAX* simulations, that I will refer altogether with the acronym *"NA"*, feature the same ocean-atmosphere coupling region, specifically the Tropical Atlantic, but have different horizontal resolutions of REMO. The *NA* simulations cover a period of 32 years from January 1980 to December 2012, for which monthly mean values are made available. The fourth simulation, which I will address with the acronym *GI3*, has the coupled ocean-atmosphere domain in the Arctic region (North Atlantic and Arctic Mediterranean), and covers a period of 85 years of from January 1920 to December 2005, of monthly mean simulated values.

Table 1 Characteristics of the simulations used in this study. The main differences in the simulations is the atmospheric resolution of the REMO part of the model ROM, the coupled domain especially between the "NA" simulations and GI3 and the period in which observations are taken.

Characteristics	NAS	NAT	NAX	GI3
Atmospheric Resolution	0.25°	0.5°	1°	1°
Coupled area	Tropical Atlantic	Tropical Atlantic	Tropical Atlantic	Artic region
Period	1980-2012	1980-2012	1980-2012	1920-2005
Observations	Monthly	Monthly	Monthly	Monthly

The difference in the atmospheric resolution in the *NA* simulations allows to identify different responses of the ocean to atmospheric changes that comprise different levels of detail. Particularly, two simulations - *NAS* and *NAT* - have a lower atmospheric resolution that only allow to simulate ocean-atmosphere interactions at large scales. *NAX*, on the contrary, has a higher atmospheric horizontal resolution that allows to simulate ocean- atmospheric coupling accounting for small-scale features of atmospheric variability. Moreover, the differences between the *NA* simulations and the *GI3* are useful to underline different contributions to SPG variability. Specifically, the contribution of fresh and cold water masses from the Artic and Nordic Seas on one side and the contribution of salt and heat transport to and within the SPG basin on the other.

The output from the four transient simulations has been manipulated as follows. First, I selected the SPG basin area to which all the variables are referred to. This area extends between the western

coast of the US to the eastern part of Europe as its western and eastern boundaries, respectively. The norther boundary is described by the southern part of Greenland, while the southern one coincides with the upper part of the Norther Tropical Atlantic, which therefore includes the effect of the Gulf stream in the SPG basin. The area weighted mean for the SPG index and the driving variables has been computed for all grid points in the selected domain in order to obtain a spatially averaged time series over the SPG area. A constant area weight for all the grid cells was used to perform the mean. Additionally, I use time series for the AMOC index and for meridional oceanic heat transport at certain latitudinal sections and depth, which are provided as standard output of the model. These series are a collection of daily observations, so I first computed a monthly means in order to reconstruct the same dataset of monthly observations used for the SPG index and the selected variables.

2.2 - Description of the driving variables

The SPG variability been associated mainly to two factors: (i) changes in the wind forcing component, mainly as a response to large-scale atmospheric variability linked to the NAO, i.e., the dominant mode of Northern Hemisphere atmospheric variability, and (ii) differences in surface buoyancy fluxes. In this thesis I mostly concentrate on the second factor, which highlights internal ocean dynamics within the SPG basin related to upper ocean properties. In order to explain the influence of buoyancy fluxes on the SPG variability, I used as driving variables Sea Surface Temperature (SST), Sea Surface Salinity (SSS), Density, and Total Fresh Water Fluxes (TFWF). To account for sea ice dynamics, I considered changes in the Sea Ice Fraction in the Denmark Strait region. Finally, to investigate the interactions between the SPG strength and the AMOC and heat transport, I used indices for the AMOC at different vertical levels and for meridional oceanic heat transport at the surface. A complete description of the variables is given in the following subsections.

2.2.1 – An index for the SPG variability

In the present study, the index used to describe the simulated SPG variability on interannual to decadal time scale, during the last century, is the absolute value of the ocean barotropic mass streamfunction. Note that the mean barotropic streamfunction in the area, hence the original values of the index, are composed by negatives values since the SPG has a cyclonic circulation pattern. This index basically represents the mass of water transported between any two points in the ocean at a given time period. This measure is commonly used within the modeling community (e.g. Eden and

Willebrand 2001; Lohmann *et al.*, 2009) to describe the evolution and dynamics of the SPG and ocean circulation (e.g. Marzocchi *et al.*, 2014).

2.2.2 – Buoyancy fluxes

Within the North Atlantic, changes in the strength and extent of the SPG have been linked to changes in the advection of water masses from the Tropical Atlantic, Nordic Sea and Arctic Ocean (Häkkinen and Rhines, 2009) and changes in their properties (e.g. Holliday *et al.*, 2008; Johnson *et al.*, 2007). In particular changes in the ocean properties in the Subpolar basin, have been associated to changes in the NAO phase, as have been already stated, and the East Atlantic Pattern (e.g. Cayan, 1992; Hurrell et al., 2013), especially in relation with changes in heat fluxes, fresh water fluxes, SST and SSS. In the present study I look at the relationship between SPG variability with changes in surface temperature, salinity and density. Altogether these processes are referred to as buoyancy forcing, which are among the main drivers of changes in the overturning circulation. The heat and freshwater fluxes at the ocean-atmosphere surface where not used here due to unresolved data inaccessibility.

SST and SSS indexes have been calculated as smoothed gridded time series and as spatially averaged time series over the SPG basin. Unfortunately, the model does not output density values. Thus, this variable has been calculated using a linear approximation of the equation of state (1), that for theoretical and practical purpose is approximated following Talley *et al.* (2011) as follows:

$$\varrho \approx \varrho_0 + \alpha(T - T_0) + \beta(S - S_0) \qquad (1)$$

Where ϱ_0, T_0, S_0 are arbitrary constant values of ϱ, T and S that are usually chosen as the mean values of the region being modelled. The coefficients α and β are the *thermal expansion coefficient* (K^{-1}) that express the change in density for a given change in temperature and the *haline contraction coefficient* (psu) that represents the change in density for a given change in salinity, respectively. Full tables of values are given in UNESCO (1987), but in the majority of case it is taken that $\alpha = 1.67 * 10^{-4}\ K^{-1}$ and $\beta = 0.78 * 10^{-3}\ psu$ (Mamayev, 2010). The constant ϱ_0 has been calculated as the mean value over the SPG basin for the total period of time. Total fresh water fluxes (TFWF) (m/s) have been calculated as the sum of solid and liquid component over the SPG basin while Sea ice Fraction area in the Denmark Strait region. Both variables have been calculated as smoother gridded and weighted averaged time series.

There is a strong interconnection between all these variables. Anomalous freshwater input into the North Atlantic and adjacent Nordic Seas, for instance, is considered critical for the variations in the

SPG basin (Born and Mignot, 2012). These anomalies can be imposed externally onto the ocean circulation as ice sheets melt or by an anomalous increase in the advection of sea ice. The internal variability of the circulation itself can nevertheless lead to the occurrence of these anomalies (e.g. Delworth *et al.*, 1993; Pohlmann *et al.*, 2004; Jungclaus *et al.*, 2005). The SPG circulation was indeed found to redistribute freshwater anomalies in the North Atlantic and Nordic Seas (Hátún et al., 2005; Wu and Wood, 2008) and to produce salinity anomalies especially in the Labrador Sea region (Delworth et al., 1993). By this, Lohmann *et al.*, 2009 hypothesized that these mechanisms can potentially decouple the ocean circulation from the atmospheric forcing and thus develop independently. In particular, Levermann and Born, 2007 have conceptualized these characteristics of the buoyancy-driven gyre circulation as a series of feedback mechanisms allowing for a bistability in the SPG, where it is at the center of three positive feedback loops. Accordingly, a stronger SPG transports more saline sub-tropical water into the SPG basin a process called salt feedback. This increases the density gradient between the SPG center and the relatively exterior boundary of the gyre. This leads to a sea surface elevation drop caused by a pressure adjustment in the water column contributing to strengthen the gyre. This intensifies the isopycnal mixing, i.e., a mixing between points that have the same density, that successively results in cooling and further increases the density of the SPG center and therewith its strength (process known as temperature feedback). This study by Born and Levermann, 2007 means to present a possible mechanism for a multistability of the subpolar gyre system based on large-scale ocean circulation. First, a stronger gyre transports more tropical saline water into the subpolar region, as opposed to the Nordic Seas. This result is consistent with high-resolution model simulations which exhibit a decreased salinity transport towards the Nordic Seas when the SPG is strong (Hátún *et al.*, 2005). Compared to a weaker gyre, less tropical waters are transported to the Nordic Seas, more of it recirculates in the SPG, making the center saltier. This increases the density gradient between the gyre and the relatively light exterior. Consequently, the sea surface elevation drops, and the corresponding geostrophic response strengthens the circulation (internal salinity feedback). The bottom pressure is practically unchanged. Secondly, a stronger SPG results in stronger outcropping of isopycnals in the center of the gyre. Therefore, heat is mixed more efficiently to depth and out of the center of the SPG which results in a cooling there. This again increases the core density of the gyre and therewith its strength (internal temperature feedback). In addition to these self-sustaining internal feedbacks, there exists an interaction with the flow over the GSR. A stronger SPG reduces Atlantic inflow into the Nordic Seas. More water downwells south of the GSR, less overflows the ridge. As a consequence, waters at the northern rim of the gyre (south of the ridge) get lighter, because they are fed by relatively light water

that is formed south of the ridge as opposed to the dense overflow waters. This increases the density gradient across the gyre and enhances its strength (positive external feedback). The causal chain of events in the simulations is related to the three described feedbacks. The first application of the positive freshwater anomaly causes an immediate reduction in overflow strength and triggers the external positive feedback. The successive increase in SPG volume transport affects the two positive internal feedbacks and causes the main increase in gyre strength. The negative freshwater anomaly shows the same succession of events, only the overflows are enhanced in response to the densification of the surface water and the external feedback is triggered negatively, leading to a reduction in SPG strength. Differences among ocean properties in the eastern and western basin are also triggers of SPG variability. For instance, the difference density between the east and west part of the basin caused by anomalous fresh and cold water masses from the Arctic in the Labrador Sea combined the a westward reduce transport of salt by the IC, due to a weaker state of the SPG lead to changes in deep water formation in the Labrador that thus contribute to sustain a weak SPG state. On the contrary, cooling in the Labrador Sea region enhances strong vertical mixing contributing to an increase of dense water in the gyre center that strengthens the SPG circulation (Born and Stocker, 2014). In the ensemble evaluation of the results we thus expect to see differences in the relation between SPG variability and the selected driving variables as well as difference between the gyre center and its boundaries.

2.2.3- AMOC and Meridional heat transport

For the AMOC I used as an index the *ocean meridional overturning streamfunction* that have been calculated for the Atlantic Ocean at different vertical level. The data where a collection of daily simulations, so I computed a monthly mean to have monthly observations. I decided to select three different level: surface (0m), upper level that for *NA* simulations is at 524m depth, while for GI3 is at 520 m, and a deep level at 1024m for *NA* simulations and 1020m for GI3. The last one can be considered, at 30°N as the maximum value that the AMOC can have. For the Heat transport I used as an index the ocean *implied heattransport* in the Atlantic Ocean region at the surface for the four transient simulations. The North Atlantic Meridional Overturning Circulation (AMOC) is an important and active component of the climate system (Rahmstorf, 2003). The connection between SPG circulation and AMOC happen along the NAC, that represents the upper branch of the AMOC, and contribute to transport large amounts of heat and salt towards the poles. The northward transports of salt is critical component for the formation of dense water, thus deep convection, in the Labrador

and the Nordic Seas (Furevik *et al.*, 2002). This dense water formed in the northern part of the SPG basin flows southward trough the Deep Western Boundary Current (DWBC) that thus compose the lower branch of the AMOC. As suggested by paleorecords (e.g. Broecker, 1997) and demonstrated by numerical studies (e.g. Manabe and Stouffer, 1999; Eden and Willebrand, 2001), the AMOC is closely related to the SPG climate state variations and vice versa. Specifically, one of the main elements of the lower branch of the AMOC is the LSW (Pickart *et al.*, 1996), that is generated especially in the winter season due to enhanced heat loss to the atmosphere and subsequent deep mixing. SPG is closely linked to deep convection in the Labrador Sea (e.g. Häkkinen and Rhines, 2004) thus the importance of SPG variability in producing changes in the AMOC strength (Böning *et al.*, 2006). Moreover, monitoring possible changes in the AMOC, especially whether the SPG index is highly correlated with the AMOC transport and the possible threat and consequences of anthropogenic climate changes can have on the connection between these two large scales current system (e.g. Hirschi *et al.*, 2003). Finally, the meridional heat transport is principally driven by SPG shift (e.g. Moreno-Chamarro *et al.*, 2016). When SPG is in a weaker state, also the heat transport is reduced, thus a small amount of upper-ocean heating reaches the center of the SPG basin. As a consequence, a small amount of heat is transported by toward the eastern part of the basin to the Nordic Seas. The heat accumulates at mid-latitudes especially in the eastern part of the basin (along the NAC) producing a strong decrease in the SST of the western basin (Moreno-Chamarro *et al.*, 2016).

3- Statistical methods

This section describes the main statistical analyses performed in the study of the SPG variability within the four transient simulations. The statistical methods make use of time series analysis, lead-lag correlation and linear regression and wavelet analysis. All the analyses have been performed using the software R studio (http://cran.r-project.org/). This tool has been selected for its great "breadboarding" system, for its ability to solve moderately large problems and for it holds a big open source community.

First, time series for the SPG index for each simulation has been created. The series are weighted mean calculated in the subpolar basin between 45 – 65 °N and 60 – 10 °W. Time series analysis is a common method to analyze the behavior and variability of a process through time. In time series analysis we are interested in the characteristics of the time evolution of a physical quantity, which is a central aspect for the characterization of climate variability. Time series are composed by different components: trend, seasonality and noise that interact in different ways. Usually, phenomena with a

particular frequency are isolated so that all the variables have been filtered to remove the seasonal cycles that are not of interest. In order to filter out the high-frequency variability of the series, a Kernel smoothing has been applied. This is a type of moving average smoother which uses unequal weights to extract the smoothed values between the neighboring observations. In the correlation and linear regression analysis the time series of the selected driving variables have also been smoothed and desonalized. The decomposition of the time series was performed with a Loess seasonal decomposition where the trend component is estimated by smoothing the desonalized time series and seasonality is estimated by smoothing the seasonal sub-series.

The driving variables (SST, SSS, density, TFWF, Sea ice area fraction, AMOC and HEAT) have been created within the subpolar basin, defined as the region between 45 – 65 °N and 60 – 10 °W. For the *NA* simulations the series comprise the period from January 1980 to December 2012, while for the GI3 simulation from January 1920 to December 2005. Smoothed annual anomalies have also been created for the SPG index and the driving variables, as the difference between the mean value over the total period of time (32 years for *NA* simulations and 85 for GI3) and the mean annual values in each year. The correlation between the time series has been computed mostly visually especially looking at the annual anomalies of the different parameters further supported by a Pearson correlation coefficient.

The spatial correlation and linear regression analyses between the SPG strength and selected driving variables are meant to explore possible causes of SPG variability and investigate their robustness (or lack thereof) among the three ensemble simulations *NA*. Together with wavelet analysis these are aimed at identifying robust precursors of SPG variations. These analyses will also reveal whether the dominant SPG mechanism in the different simulations is the same notwithstanding differences in the emerging SPG behaviors. In the following, the negative values of the lag k mean that the SPG leads changes in the driving variables, while for positive values of k the SPG lags. I decided to use values for k in the range from -36 to +36 months, sampled every 12 months, i.e. we can see yearly changes in the long-term relation, as well as in the range from - 8 to +8 months, sampled every 2 months, to highlight sub-seasonal changes. All correlations and regressions shown in the figures in the present thesis are significant above the 95% confidence level (grid points where the correlation is not significant are color white).

The wavelet analysis was performed using the *WaveletComp 1.1* R package (by Roesch and Harald), to show relationships at different climatic states (Brauch and Gerdes 2005; Lohmann *et al*., 2009). The wavelet analyses comprise a cross-wavelet analysis between annual anomalies of the SPG index and the driving variables. The same procedure has been used when computing the relation between

the SPG index, the AMOC and heat transport. The wavelet analysis method of the R package compares the frequency structure of two series using the Morlet wavelet. It is built on a Gaussian-windowed sinusoid, the Gabor transform, which was introduced in 1946 by Gabor to decompose a signal into its frequency and phase content as time evolves. The Morlet wavelet transform of a time series is thus defined as the convolution of the series with a set of "wavelet daughters" generated by the mother wavelet by translation in time and scale. First, I compute the cross-wavelet between two series, in order to compare the frequency contents of the two series to draw conclusions about their synchronicity at certain periods and across certain ranges of time. Then, I analyzed the phase difference between the series, in order to assess whether the two series are synchronized in the time domain in terms of the instantaneous or local phase difference of any periodic component of the first series with respect to the correspondent component of the others. In the interpretation of the results of the graphical representation of the phase difference between the series, an absolute value less (larger) than π/2 indicates that the two series move in phase (anti-phase, respectively) referring to the instantaneous time as time origin and at the frequency (or period) in question, while the sign of the phase difference shows which series is the leading one in this relationship displayed as arrows in the image plot of cross-wavelet power as shown in Figure 3 (Aguiar-Conraria and Soares, 2011). Finally, in the plot of the cross-wavelet power, the time axis the years are counted as time unit i.e. the first year "*1*" correspond to 1980 and so on.

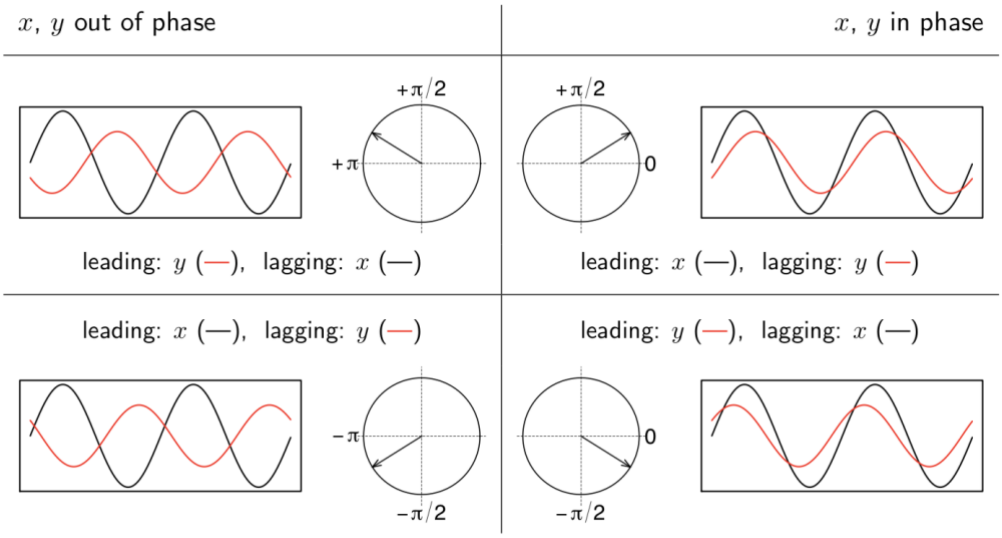

*Figure **3** Illustration of the range of possible phase differences and their interpretation in the style of a diagram by Aguiar-Conraria and Soares 2011, taken from http://www.hs-stat.com/projects/WaveletComp/WaveletComp_guided_tour.pdf*

SECTION C: RESULTS

This section describes the main results from the statistical analyses on the four transient simulations. In the first paragraph I first will describe the output of the time series analysis on the *NA* simulations, which cover the same time period, underling the differences among them. Secondly, I will describe the results from the fourth simulation *GI3*, which covers a different time period compared to the *NA* simulations. Conclusively, a comparison between the four simulations. A second paragraph follows that illustrate the results from the lead-lag correlation and linear regression analysis and wavelet analysis in particular aiming at identifying robust precursors of SPG variations. These analyses are meant to explore possible causes of SPG variability and investigate their robustness (or lack thereof) especially among the three ensemble simulations *NAS*, *NAT* and *NAX*. These analyses will indeed reveal whether the dominant SPG mechanism in the different *NA* simulations are the same notwithstanding differences in the emerging SPG behaviors (i.e., the temporal evolution of the SPG index in the different simulations). The last paragraph describes the relationships between the SPG variability, AMOC intensity and oceanic heat transport.

As a general observation, in many cases the *NAS* and *NAT* simulation show a similar behavior and for this reason I decided to show only the results of *NAS.*

4.1- The variability in the SPG index

I used an index for the SPG strength to describe its variability on decadal and longer time scales in four transient simulations. The climatological value (i.e. the period means) of the mass barotropic streamfunction in the SPG core region is negative in all the simulations, which indicates a cyclonic circulation. The SPG index used here, is the absolute value of the mass barotropic streamfunction spatially averaged in the subpolar gyre basin between 45 – 65 °N and 60 – 10 °W and further smoothed with a Kernel smoothing over the whole period.

Please recall that, in the interpretation of the ensemble results, the occurrence of differences among the simulations in the SPG evolution is associated with internal climate variability (the “random” variability that arises spontaneously due to the nonlinear and chaotic character of the system and is expected to be different in each simulation), whereas consistent behavior reveals the predominance of the effects of external forcing.

The long term-tendency of the SPG index in the *NA* simulations show some differences (Figure 4). Qualitatively, two simulations (*NAS* and *NAT*) have the same overall behavior that is also confirmed by a high correlation coefficient (Spearman correlation coefficient of 0.89, $p < 0.05$). SPG evolution,

remains rather constant in the first ten years until the 90's successively develops in an increasing trend, defined as the as the slowly varying component determining the time series level without the period or seasonal components, that culminates with a maximum pick around 1997 successively followed by a decreasing trend that lasts until 2007.

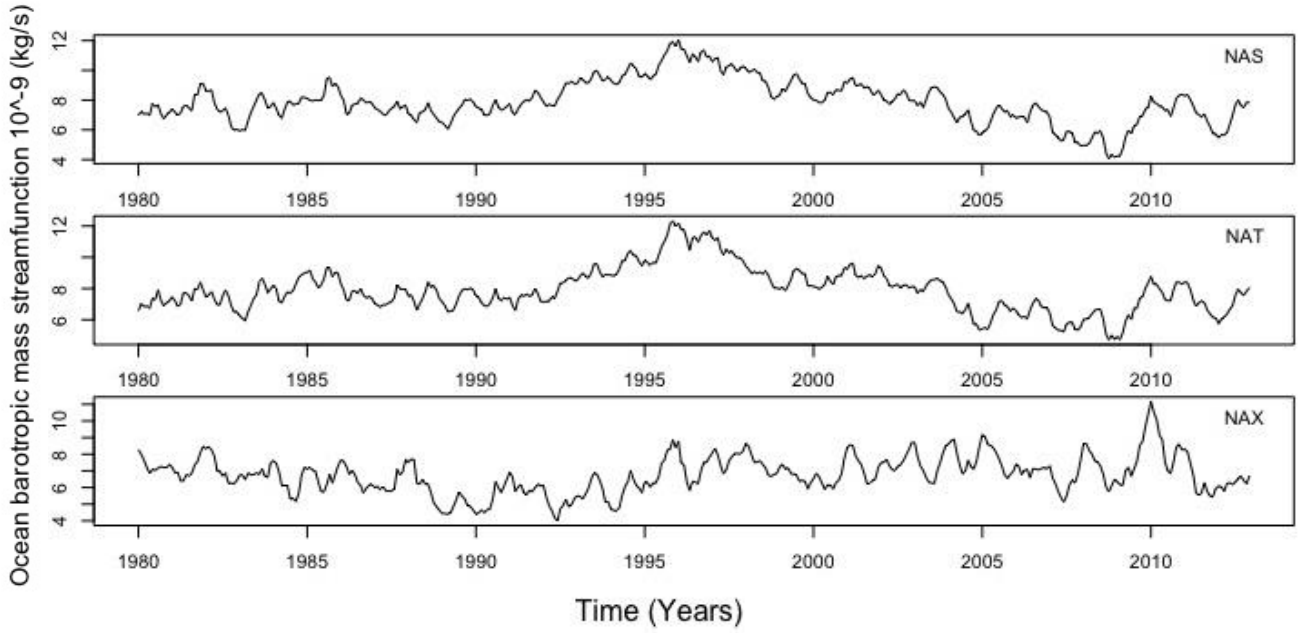

*Figure **4** Index for the SPG variability: black solid lines are the corresponding smoothed values of the SPG index spatially averaged between 45 – 65 °N and 60 – 10 °W between 1980 and 2012 in three transient simulations (NAS, NAT and NAX) with a different atmospheric resolution.*

The decreasing trend, thus weakening of the SPG during this period of time, has also been found both by direct observations (e.g. Häkkinen and Rhines 2004) or models result (Böning et al., 2006). All results agree notwithstanding the index has been calculated differently in different studies (e.g. using the Sea Surface Height values (SSH). The *NAX* simulation shows an apparently different evolution from the first two, which is further stressed by low correlation coefficients for *NAS* (Spearman correlation coefficient of 0.33, $p < 0.05$) and *NAT* (Spearman correlation coefficient of 0.37, $p < 0.05$). This simulation shows a more stationary evolution, characterized by a slight decrease around 1995 followed by a slight increase around 1997. Similarly, this simulation exhibits the interannual variability, that here appear particularly prominent around 1990 with a decrease in the SPG index, and with a pick around 2010. Both features do not emerge in *NAS* and *NAT*, as strong as in NAX.
Generally, the three simulations are able to reveal the interannual variability that characterized SPG index but *NAX* doesn't show any significant and long-lasting shifts associated to a transition from/to a weaker/stronger state are shown as in *NAS* and *NAT*.

The fourth coupled simulation, *GI3*, covers a longer period of time (85 years) and is characterized by an initial increasing trend starting during the 1920s, a maximum in the late 1930s and a decrease until around 1950s (Figure 5a).

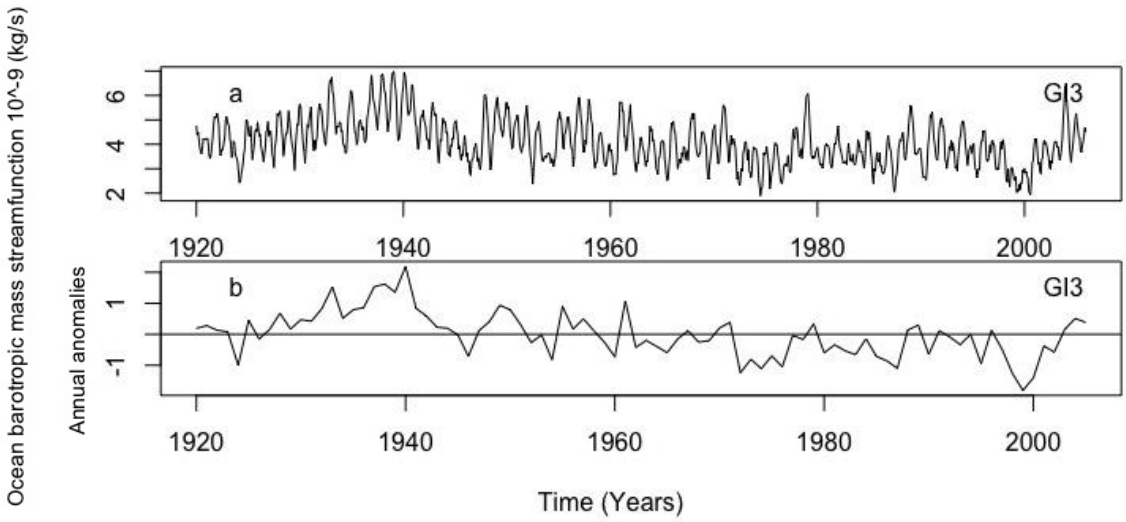

*Figure **5 a** Index for the SPG variability: black solid lines are the corresponding smoothed values of the SPG index spatially averaged between 45 – 65 °N and 60 – 10 °W between 1920 and 2005 in GI3 simulation. **b** Smoothed annual anomalies calculated between 1920 and 2005 throughout the SPG basin*

Then, an almost stationary period starts, with values of the SPG index around 4 *10^9 kg/s, which is interrupted by a weakening around the mid 70's. A second noticeable weak anomaly can be identified at the end of the XX century, which can be better appreciated in the annual anomalies of the SPG index (Figure 5b). This simulation also reveals prominent decadal variability between 1930 and 1940 and inter-annual variability, that is particularly revealed between 1950 and 1960. This could be a consequence of the Arctic warming that has produced a warming air temperature averaged for the 1940s with some 1.7°C (2.2°C for the winter half of the year) relative to the 1910s (e.g. Johannessen et al., 2004).

An interesting difference among the four simulations concerns the distributional range of SPG values that in *GI3* is determined by a lower mean (around 4 $*10^{-9}$ kg/s for *GI3*, around 7 $*10^{-9}$ kg/s for *NAS* and *NAT* and 6 $*10^{-9}$ for *NAX*) but larger amplitude of the seasonal signal compared to the *NA* simulations (Figure 6). Interestingly, the climatological spatial pattern of the SPG appears similar between *NAS*, *NAT* and *NAX*, with maximum values for SPG index in the center of the gyre and in western part of the basin (very clear in *NAX*). Nevertheless, the simulations show some differences concerning the size and expansion of the western branch of the SPG, larger for *NAX* and thinner in

NAS and *NAT*. Differently, in *GI3* the shape of SPG is less clear and the index has higher values just between the western and eastern shelves of Greenland while in the rest of basin the values are considerably low. Increasing the model resolutions of the REMO part leads to a slight decrease of the absolute transport in the subpolar basin (differences between absolute mean values ranges in *NAT*, *NAS* and *NAX*), as changing the coupled atmospheric-ocean part (as can been seen in *GI3*).

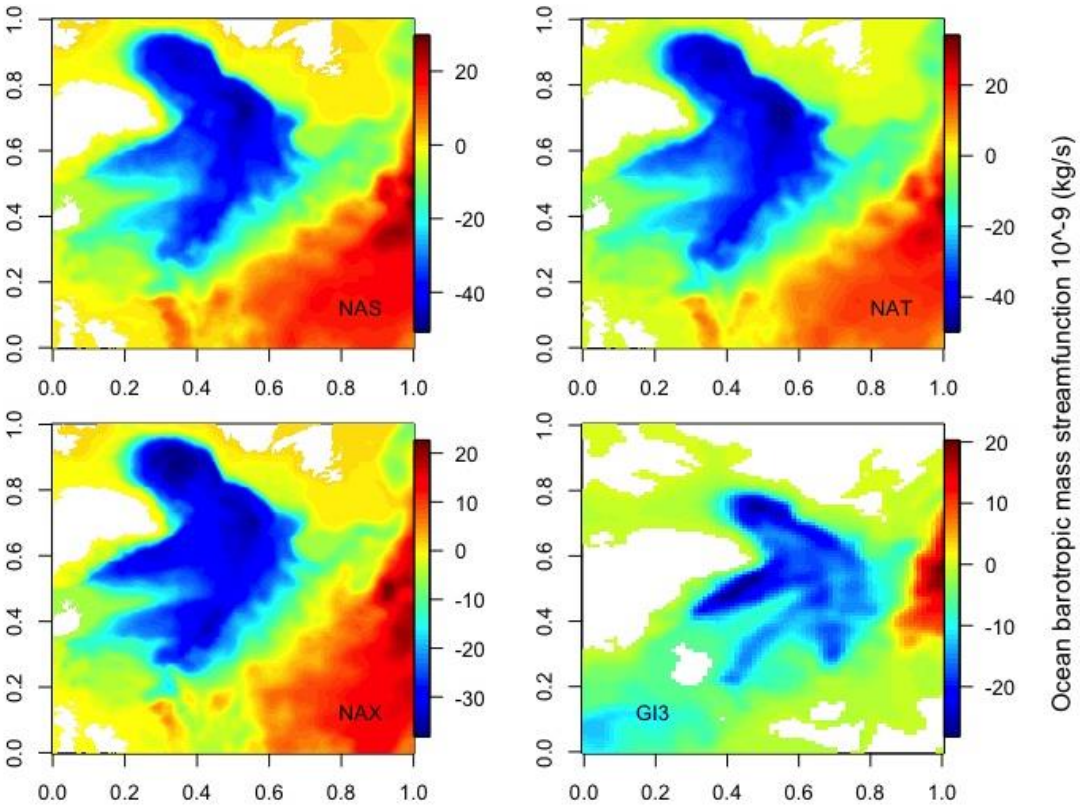

*Figure **6** Climatological mean of the mass barotropic streamfunction in four transient simulations NAS, NAT, NAX and GI3 throughout the SPG basin, between 1980 and 2012 (NAS, NAT and NAX) and between 1920 and 2005(GI3). Negative values in the SPG core region indicates a cyclonic circulation while positive values characterize the anticyclonic subtropical gyre*

4.2- Mechanisms of SPG variability: comparative analysis of lead – lag correlation and linear regression and wavelet analyses in the NA simulations

This paragraph compares the results of correlation and regression analyses between the SPG strength and selected driving variables. These analyses are meant to explore possible causes of SPG variability and investigate their robustness (or lack thereof) among the three ensemble simulations *NAS*, *NAT* and *NAX*. Lead-lag correlation and regression analysis, and wavelet analysis will be used to investigate

the mechanisms of simulated SPG variability, in particular aiming at identifying robust precursors of SPG variations. These analyses will also reveal whether the dominant SPG mechanism in the different simulations are the same notwithstanding differences in the emerging SPG behaviors.

4.2.1- Sea surface temperature

The temporal and spatial variability of the SPG index in relation with SST, shows the same patterns between *NAT* and *NAS*. Particularly, *NAS* (Figure 7) and *NAT* (not shown) suggest a negative correlation in the whole basin when SPG lags. Negative correlated areas are located especially close to Denmark strait and in the southern boundary of the SPG. This suggest that local decreasing in SST values, leads to a weakening of the SPG strength. Accordingly, for instance cold upper temperature in the Labrador Sea can produce and increase of the upper-ocean density.

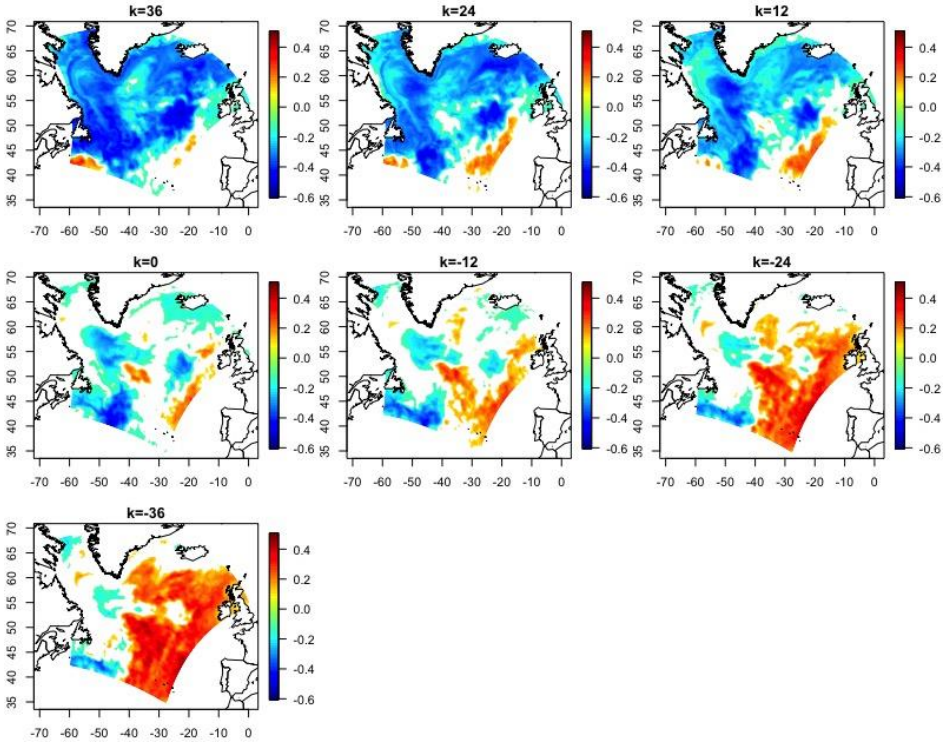

Figure 7 Yearly changes in the long-term lead-lag correlation between SPG variability and SST in the subpolar basin for NAS simulation between 1980 and 2012. Only significant correlated areas above the 95% confidence level are shown. Positive values of lag k mean that SPG lags while the negative values of the lag k mean that the SPG leads changes in the SST.

This consequently, induce a resume of deep water that enhance the mixing between deeper and surface waters, a reduction of the SSS in the Labrador Sea region and strengthening the SPG. On the contrary, when SPG leads there is a consistent behavior between SPG and SST changes as shown by the positive correlated areas. Indeed, a weaker (stronger) state of the SPG, for instance sustains weaker (stronger) northward surface transport of warm water through the Gulf currents. This is particularly visible in the eastern part of the SPG basin known as the intergyre-gyre region that is indeed associated with the propagation of the Gulf stream in the separation region between the Tropical Atlantic and the SPG basin. The regression analysis yields the same results from the

correlation analyses, especially in the positive linear relation between SPG variability and SST, when SPG lead, close to the intergyre-gyre region especially in the long-term relation. This area, on the contrary is shows negative values when SPG leads (Figure 8).

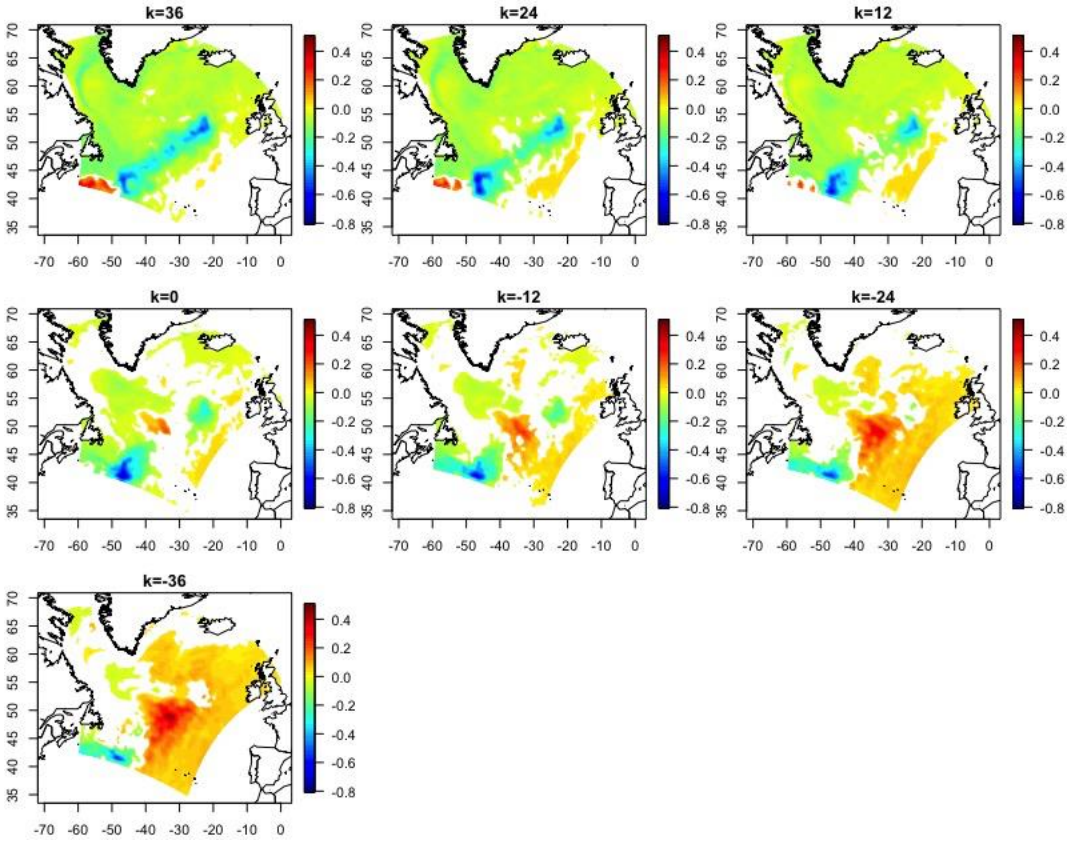

*Figure **8** Yearly changes in the long-term lead-lag regression between SPG variability and SST in the subpolar basin for NAS simulation between 1980 and 2012. Only significant areas above the 95% confidence level are shown. Positive values of lag k mean that SPG lags while the negative values of the lag k mean that the SPG leads changes in the SST.*

The NAX simulation partly confirms the negative correlation between SST and SPG in the whole basin detected in NAS and NAT (Figure 9). However, the correlations are not strong as in *NAS and NAT.* Interestingly, here we can see, when SPG leads, a positive correlation between the two variables when SPG leads, which is strong specially along the eastern and western shelves of Greenland and in Labrador Sea (in k=0). This can sustain a lower transport of heat westward, thus a decrease in the SST in these regions. The same overall behavior is shown also in the regression analysis. Interestingly, the linear regression results in the long-term changes agrees with *NAS and NAT* especially in the negative correlated area close to the intergyre-gyre region (clearly visible k=-36), even though with a relation that is weaker that the one in *NAS* and *NAT* (Figure 10)

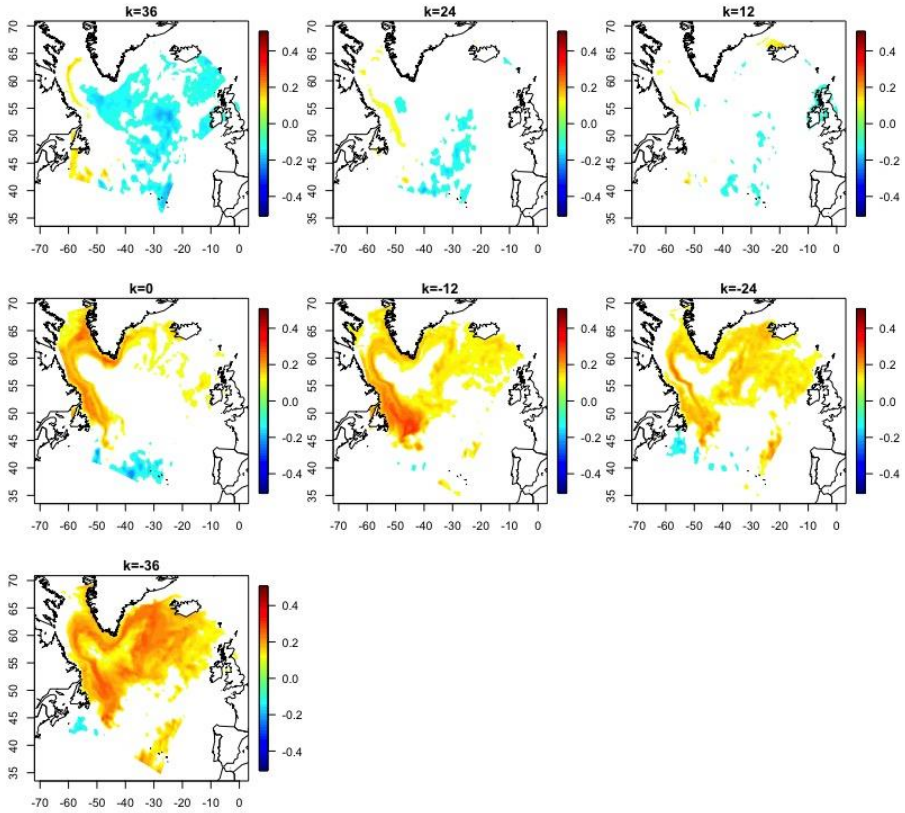

*Figure **9** Yearly changes in the long-term lead-lag correlation between SPG variability and SST in the subpolar basin for NAX simulation between 1980 and 2012. Only significant correlated areas above the 95% confidence level are shown. Positive values of lag k mean that SPG lags while the negative values of the lag k mean that the SPG leads changes in the SST.*

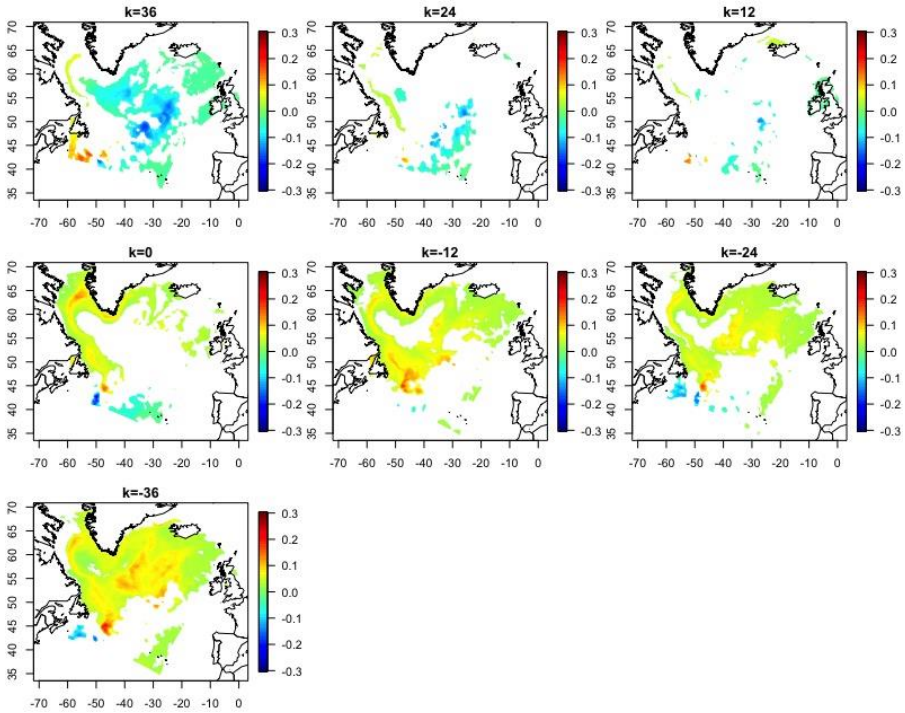

*Figure **10** Yearly changes in the long-term lead-lag regression between SPG variability and SST in the subpolar basin for NAX simulation between 1980 and 2012. Only significant areas above the 95% confidence level are shown. Positive values of lag k mean that SPG lags while the negative values of the lag k mean that the SPG leads changes in the SST.*

The wavelet analysis results are similar for NAS and NAT, where the superposition between the phase state and the cross-wavelet pawer, it shows a relation in which SPG lag to changes in the temperature especially in the period between 1990 and 2005 (Figure 11). Indeed, a major difference between the *NA* simulations is in the steepness of the increasing trend around 1995: that in NAX is characterized by a small increase in the values from a lower point to a the higher one, while in NAS and NAT this warming period is better traced with increases of almost 2.5 °C (Figure 12). This trend has been confirmed to be associated with major changes in the ocean circulation or with changes in the NAO phase that exhibit a strong phase around 1995 – (e.g. Hermanson et al., 2014).

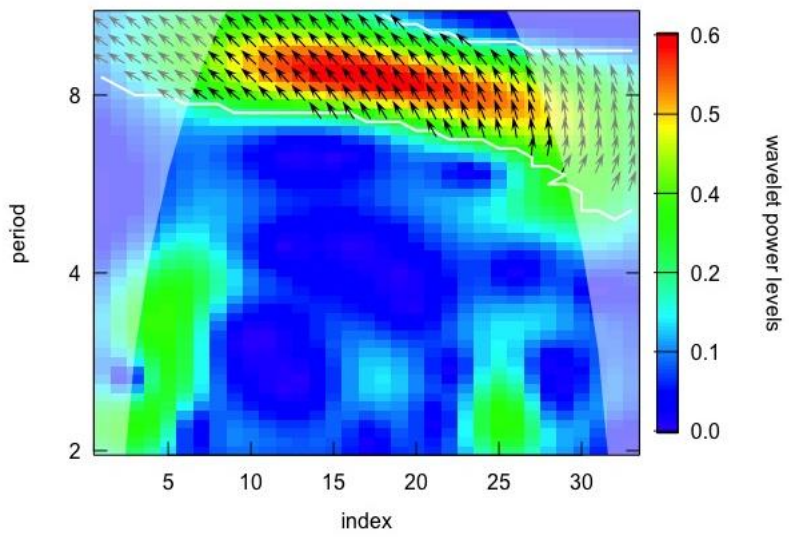

*Figure **11** Cross-wavelet power between smoothed SPG annual anomalies and SST annual anomalies between 1980 and 2012 throughout the SPG basin for the NAS simulation. The color bar indicates the relevance, red colors mean higher relevant period. The direction of the arrows indicates the lead – lag relationship between the variables, in this case SST leads.*

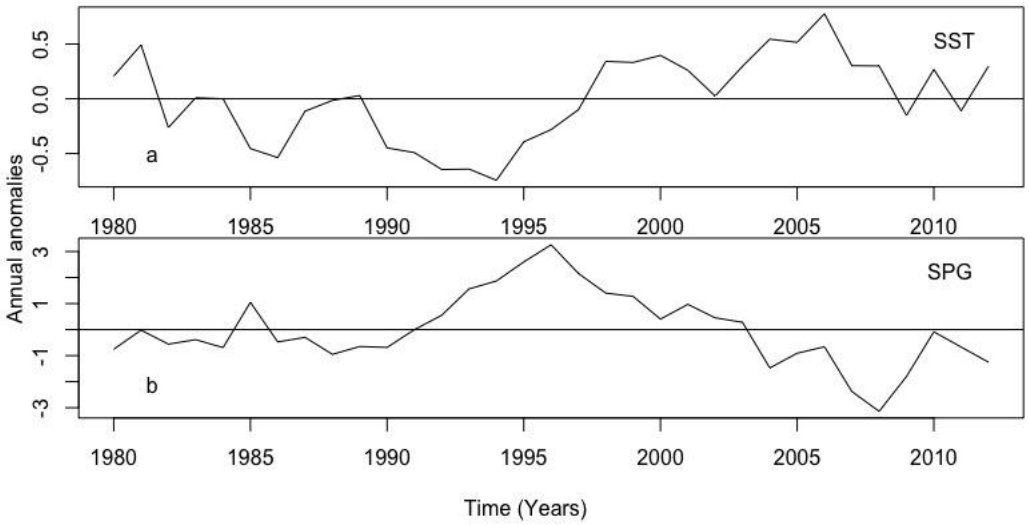

*Figure **12 a** Smoothed annual anomalies of variable SST of NAS simulation throughout the SPG basin calculated between 1980 and 2012. **b** Smoothed annual anomalies of variable SPG of NAS simulation throughout the SPG basin calculated between 1980 and 2012.*

For the *NAX* simulation, the wavelet analysis shows a different behavior compared with *NAS* and *NAT* with SPG leading in the period between 1980 – 2000 with a low power and especially between 2005-2012 with the two series are in phase (Figure 13), as well as differences in the annual anomalies (Figure 14).

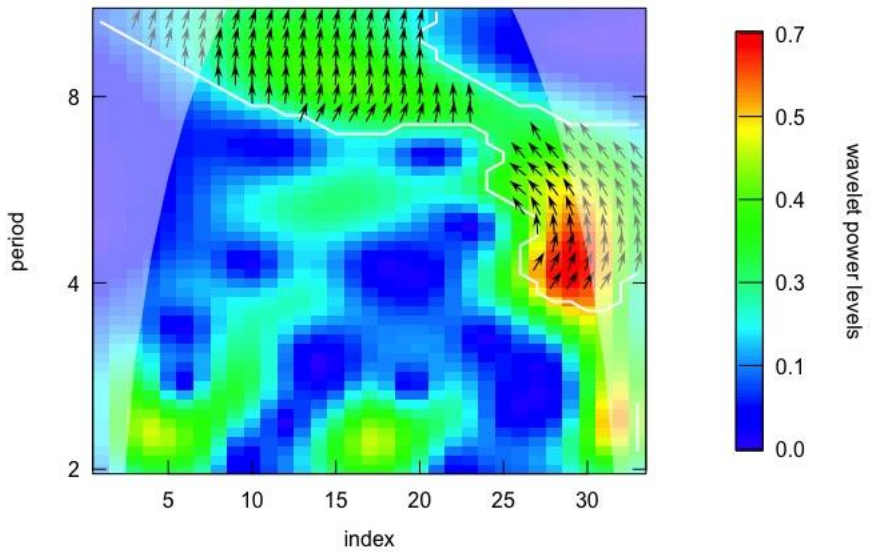

*Figure **13** Cross-wavelet power between smoothed SPG annual anomalies and SST annual anomalies between 1980 and 2012 throughout the SPG basin in the NAX simulation. The color bar indicates the relevance, red colors mean higher relevant period. The direction of the arrows indicates the lead – lag relationship between the variables, in this case SST lags.*

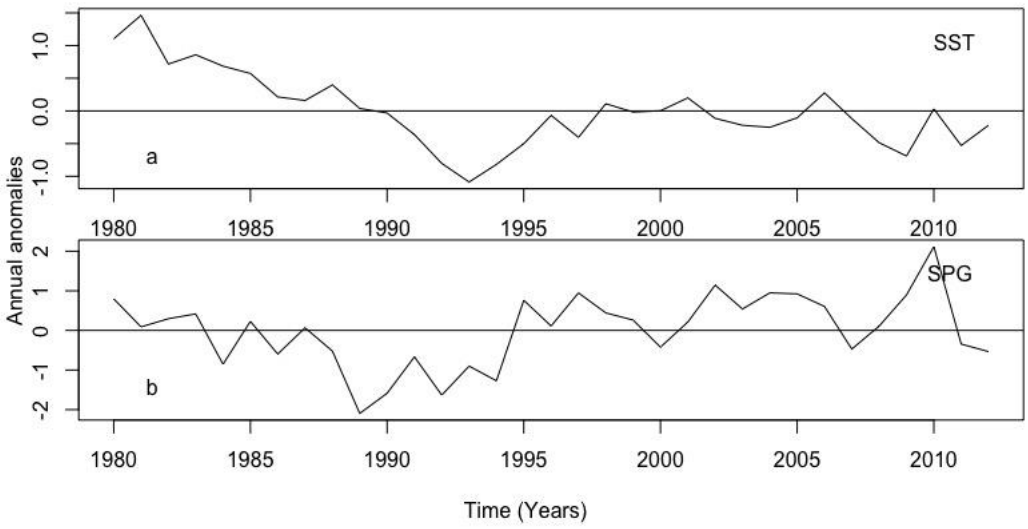

*Figure **14 a** Smoothed annual anomalies of variable SST of NAX simulation throughout the SPG basin calculated between 1980 and 2012. **b** Smoothed annual anomalies of variable SPG of NAX simulation throughout the SPG basin calculated between 1980 and 2012*

4.2.2- Sea surface salinity

There is an agreement between all the *NA* simulations, the general patterns are clearly visible in *NAS* (Figure 15) and *NAT* (not shown), less in NAX (Figure 16). Especially in the short-term variations, it is clear the difference between the gyre center and its boundaries, determined by a strong negative correlation values in the gyre center and positive at its boundaries, reflecting the same pattern found

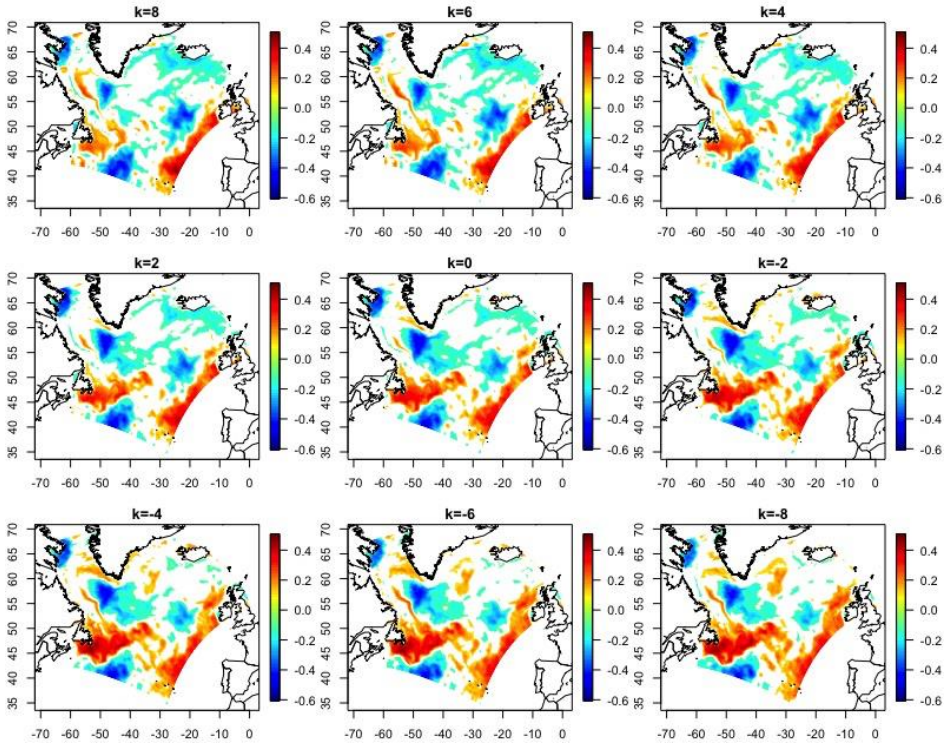

*Figure **15** Sub-seasonal changes in the short-term lead-lag correlation between SPG variability and SSS in the subpolar basin for NAS simulation between 1980 and 2012. Only significant correlated areas above the 95% confidence level are shown. Positive values of lag k mean that SPG lags while the negative values of the lag k mean that the SPG leads changes in the SSS.*

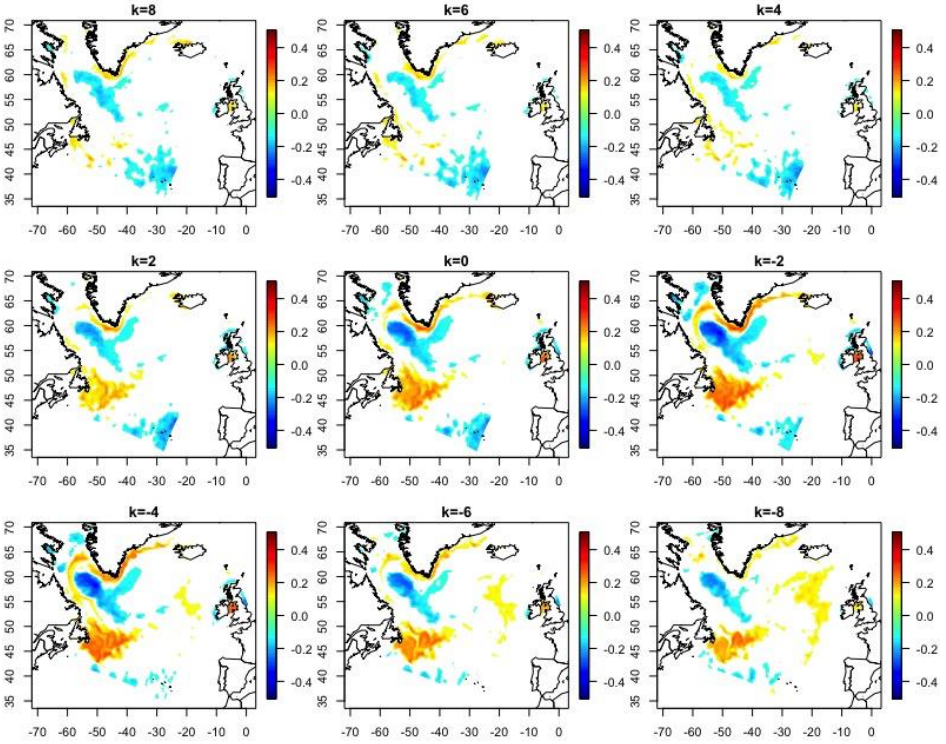

*Figure **16** Sub-seasonal changes in the short-term lead-lag correlation between SPG variability and SSS in the subpolar basin for NAX simulation between 1980 and 2012. Only significant correlated areas above the 95% confidence level are shown. Positive values of lag k mean that SPG lags while the negative values of the lag k mean that the SPG leads changes in the SSS.*

out for SST. Then, it is also possible to notice a negative correlated area near the Denmark/Fram strait when SPG lags. This is due to the fact that a higher fresh water input from the Arctic contributes to slow down the SPG, hence weakening it. Such a precursor is even clearer in the long-term relation between SSS and SPG index. The correlation pattern in the Labrador Sea is fragmented between positive and negative small areas either SPG lags or leads. Nonetheless, there is a patch of positive correlations in the center of the Labrador Sea for large lags, suggesting that salinification of the Labrador Sea is a precursor of a SPG strengthening, with time scales for this effect of up to 3 years. Finally, the results show interesting correlation patterns emerging towards midlatitudes, which may reflect the interaction between the LC and the Gulf stream that enters in the subpolar basin by the western part:

a positive correlation that strongly emerges especially when the SPG leads (clearly observable from lag= -12 to lag= -36) corresponds to transport of anomalously salty and warmer waters into the SPG. This interpretation is consistent with the known relation between a stronger phase of the SPG being associated with a strong transport of subtropical waters in the basin (Levermann and Born, 2007). Another possible explanation of the relation between SSS and SPG found here is provided by Levermann and Born, 2002, who suggest a bistability of the SPG associated to changes in the transport of saline tropical water in the basin that creates loops within the basin connected with changes in density and ocean heat release to the atmosphere. Finally, we can notice an area of negative correlations in the southern part of the basin, something that is also revealed in the regression analysis, especially in *NAS* (Figure 17) and *NAT* (not shown). It suggests a negative interaction between the subpolar gyre and the subtropical gyre: note in this regard that the main mode of gyre circulation in the North Atlantic is the so-called intergyre-gyre, which describes variations at the boundary between the two gyres linked to NAO variability (e.g., Marshall et al., 2001).

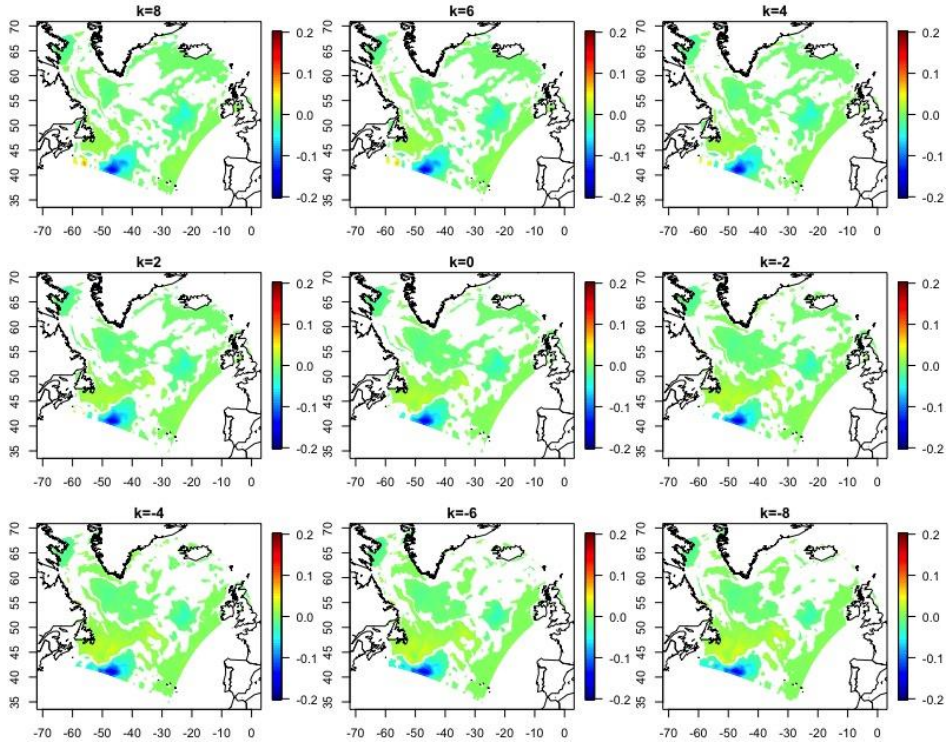

*Figure **17** Sub-seasonal changes in the short-term lead-lag linear regression between SPG variability and SSS in the subpolar basin for NAS simulation between 1980 and 2012. Only significant areas above the 95% confidence level are shown. Positive values of lag k mean that SPG lags while the negative values of the lag k mean that the SPG leads changes in the SSS.*

The wavelet analysis doesn't show similar patterns in the *NA* simulations for the wavelet analysis results. Also in this case there is a strong agreement between the *NAS* and *NAT* simulations, showing an out of phase state between 1995 and 1995 with SSS leads with a lower power, and another more significant out of phase state with SSS leads at the end of the century at lower frequency (Figure 18). The results from the *NAX* simulations agrees with *NAS* and *NAT* especially showing a period where the two series are in phase with SSS leads (Figure 19).

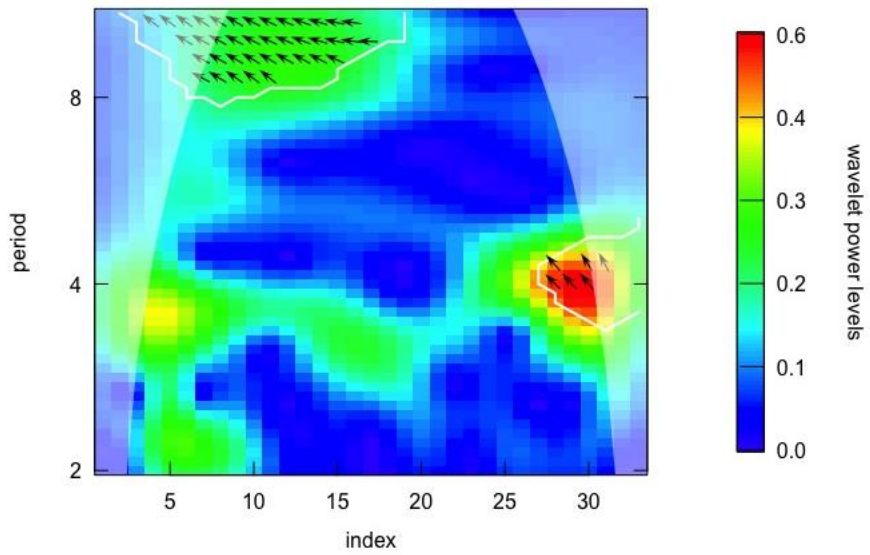

*Figure **18** Cross-wavelet power between smoothed SPG annual anomalies and SSS annual anomalies between 1980 and 2012 throughout the SPG basin in the NAS simulation. The color bar indicates the relevance, red colors mean higher relevant period. The direction of the arrows indicates the lead – lag relationship between the variables, in this case SSS leads*

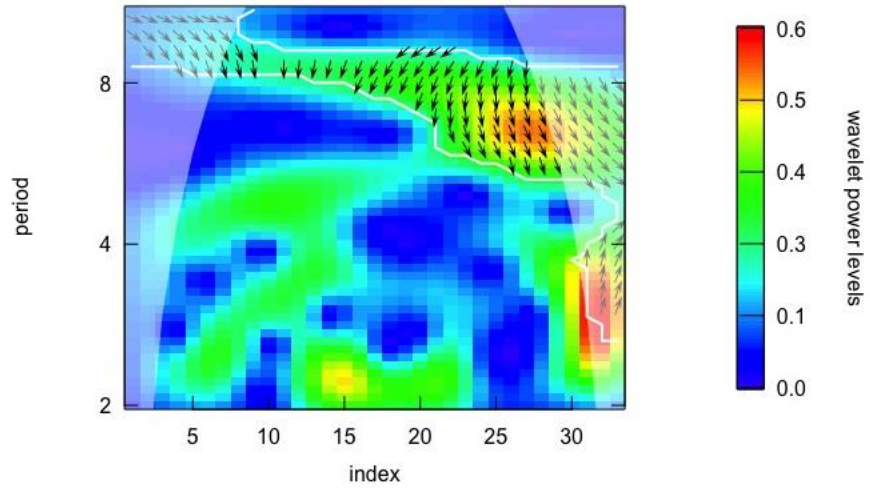

*Figure **19** Cross-wavelet power between smoothed SPG annual anomalies and SSS annual anomalies between 1980 and 2012 throughout the SPG basin in the NAX simulation. The color bar indicates the relevance, red colors mean higher relevant period. The direction of the arrows indicates the lead – lag relationship between the variables, in this case SSS leads*

4.2.3- Density

As the model output does not include values for the density, these were calculated from SST and SSS values as explained in Section 2.2.2. Therefore, these results must be taken with some caution. As said in the Introduction, the mixing and the presence of different currents (salty-warm VS fresh-cold) contribute to give action to SPG circulation pattern especially in the deep convection regions such as the Greenland-Scotland Ridge (GSR) and the Labrador Sea. To gain deeper insights into the density changes and their role for oceanic convection, these results should be further integrated with specific

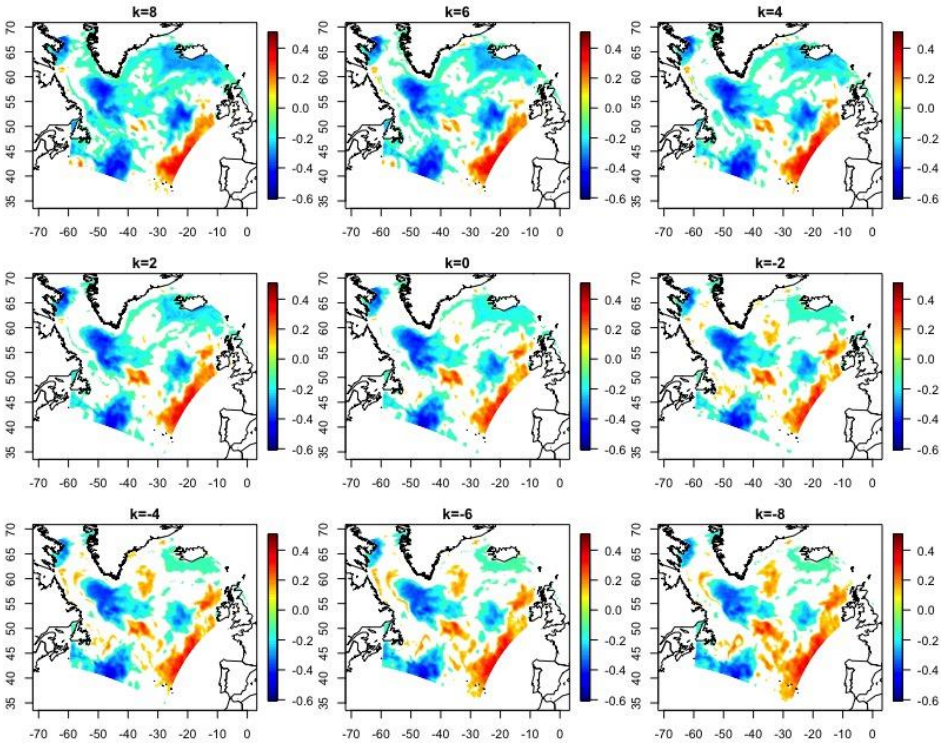

*Figure **20** Sub-seasonal changes in the short-term lead-lag correlation between SPG variability and density in the subpolar basin for NAS simulation between 1980 and 2012. Only significant correlated areas above the 95% confidence level are shown. Positive values of lag k mean that SPG lags while the negative values of the lag k mean that the SPG leads changes in the density.*

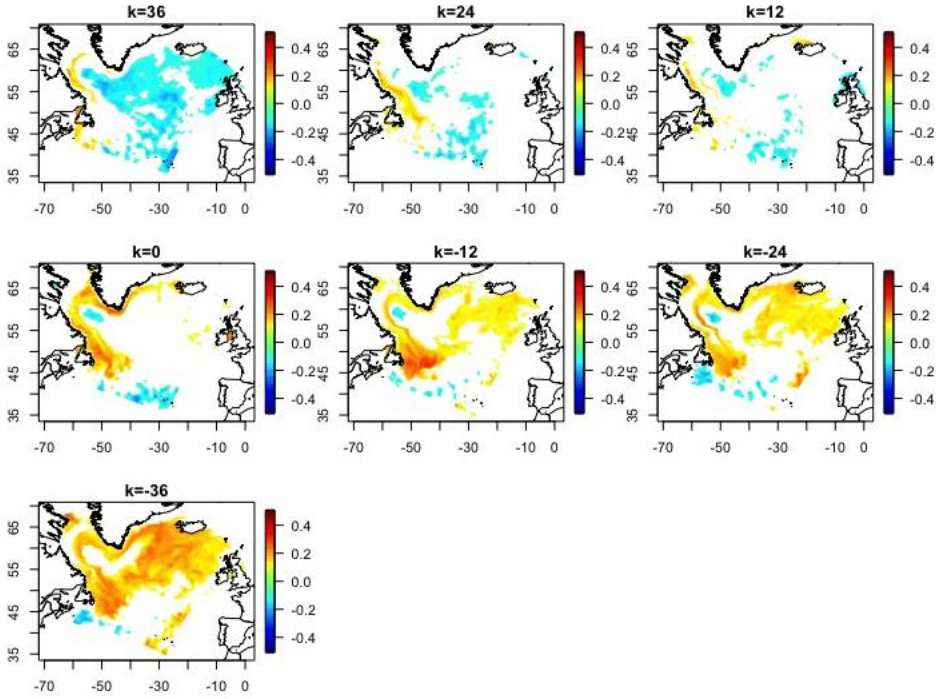

*Figure **21** Yearly changes in the short-term lead-lag correlation between SPG variability and density in the subpolar basin for NAX simulation between 1980 and 2012. Only significant correlated areas above the 95% confidence level are shown. Positive values of lag k mean that SPG lags while the negative values of the lag k mean that the SPG leads changes in the density.*

analysis in these areas, for instance including diagnostics such as the mixed layer depth as a measure of the oceanic convection. As previously said, particularly attention should be posed in the difference between the eastern and western parts of the basin, as well as local and regional variations especially in the site for deep water formation or mixing. The last aspect is quite well represented in the lead-lag correlation especially in *NAS* (Figure 20) and *NAT* (not shown) where we can see large temporal variations in the spatial pattern of the relation between density and SPG strength. Also in this case we can see the differences between the gyre centre and its boundaries when the SPG leads. Finally, the *NAX* simulation (Figure 21) clearly shows the positive correlation at the boundaries of the gyre, especially close to the GSR and in the Labrador Sea discussed above.

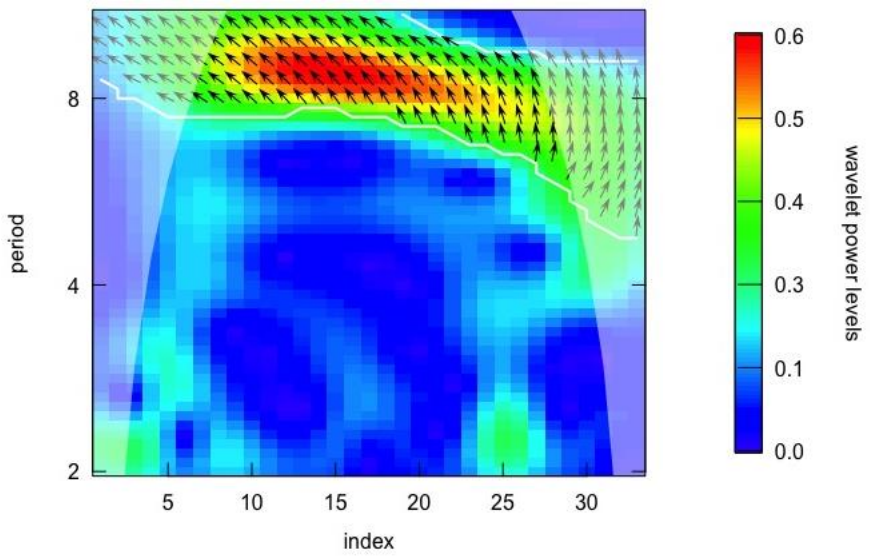

*Figure **22** Cross-wavelet power between smoothed SPG annual anomalies and density annual anomalies between 1980 and 2012 throughout the SPG basin in the NAS simulation. The color bar indicates the relevance, red colors mean higher relevant period. The direction of the arrows indicates the lead – lag relationship between the variables, in this case density leads.*

The wavelet analysis reveals, as suggested also for SSS, that for *NAS* and *NAT* the two series are out of phase with SPG lags, with a higher power, especially in the period between 1980 and 2005 (Figure 22), while the results for *NAX* are difficult to interpret since there is no overlapping between the cross-wavelet and phase plot.

4.2.4 –Total Fresh Water Fluxes

The influence of fresh water on the SPG strength is mainly expressed in the north part of the basin, and particularly in the upper Nordic and Labrador Sea, and in the Denmark Strait. There is an opposite relation between the SPG variability and TFWF within the Labrador Sea and the Denmark strait, where an increase in the freshwater flux yields a stronger and a weaker SPG, respectively. This is confirmed by the correlation analysis in the three *NA* simulations (Figure 24, *NAS* results) especially as far as sub seasonal changes are

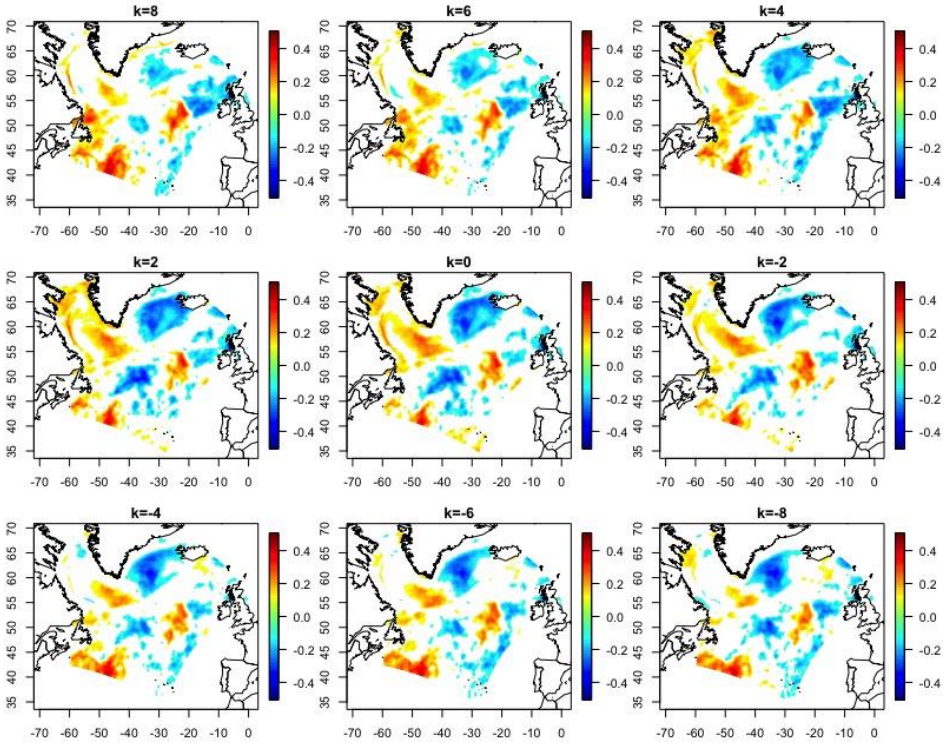

*Figure **24** Sub-seasonal changes in the short-term lead-lag correlation between SPG variability and TFWF in the subpolar basin for NAS simulation between 1980 and 2012. Only significant correlated areas above the 95% confidence level are shown. Positive values of lag k mean that SPG lags while the negative values of the lag k mean that the SPG leads changes in the TFWF.*

concerned. This can be explained by the fact that fresh waters that flow from the Arctic are strongly seasonally influenced by the amount of sea ice present during the different seasons. It is clear that there is a negative correlation in the Denmark strait when SPG leads, that means that weaker state of SPG contributes to increase the TFWF through the Denmark Strait. This has also consequences in the Labrador TFWF: larger freshwater fluxes here contribute to the surface freshening and thus sustain a weaker SPG state and this is indeed shown by the positive correlation coefficients obtained when the SPG lags ($k > 0$). The *NAX* simulation provides unclear results: they confirm the same general pattern shown in Figure 24 but the emerging features have small spatial scales, and the general pattern is patchy and difficult to interpret. For a deeper understanding of the dynamics would require more detailed analysis focused on the Labrador Sea and Denmark Strait, as well as the separate contributions of the solid and liquid on the SPG variability. Moreover, the fresh water fluxes and sea ice dynamics are strongly related with wind forcing through its effects on the evaporative and heat fluxes as well as through its active action on sea ice transport from the Arctic towards the North Atlantic. The results of the wavelet analysis are indeed quite inconclusive when performed in the whole basin recognizing the required in-depth analysis.

4.2.5 – Sea ice area fraction – Denmark Strait

There is a strong agreement between the *NA* series (Figure 25): all show prominent seasonal variations in the sea ice area, that is larger in winter than summer, as well as interannual variations. Interannual variations are very clear shown in the period between 1987 and 2000 that is characterized by an alternation of positive and negative anomalies. This period is followed by a slowly decreasing trend until the end of the series, when we diagnose a predominance of negative anomalies.

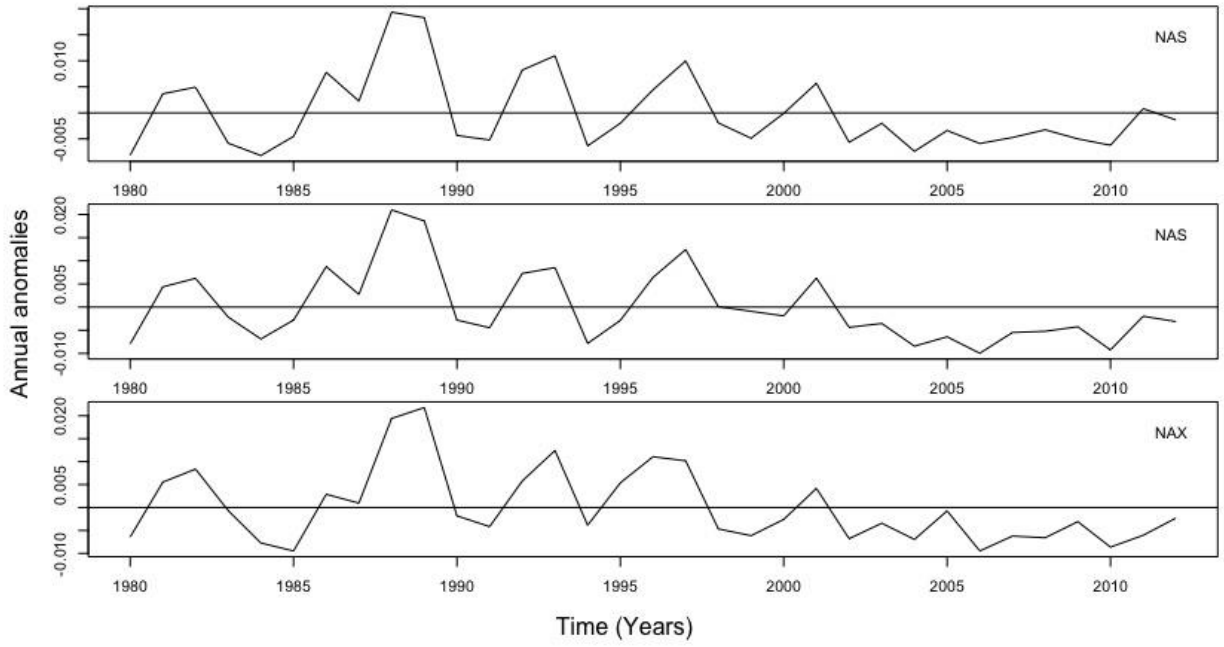

*Figure **25** Smoothed annual anomalies of variable sea ice fraction area of all NA simulations throughout the Denmark Strait calculated between 1980 and 2012.*

Previous studies, e.g. Born *et al.,* 2010, have suggested the occurrence of a link between Arctic sea ice export, extend and thickness especially in Denmark Strait and David Strait (e.g. Aagaard and Carmack 1989). This region is one of the major sources of fresh water for the Subpolar North Atlantic basin. Moreno – Chamarro *et al.,* 2016 showed that increased freshwater transport (especially in solid part) can contribute to a weakening of the SPG. The same was found by Born et al., 2010, suggesting that sea ice transport can impact especially deep convection and SPG strength. The wavelet analysis doesn't show clear results for the *NAS* and *NAT* simulation, while for the *NAX* simulation it is possible to observe an out of phase state

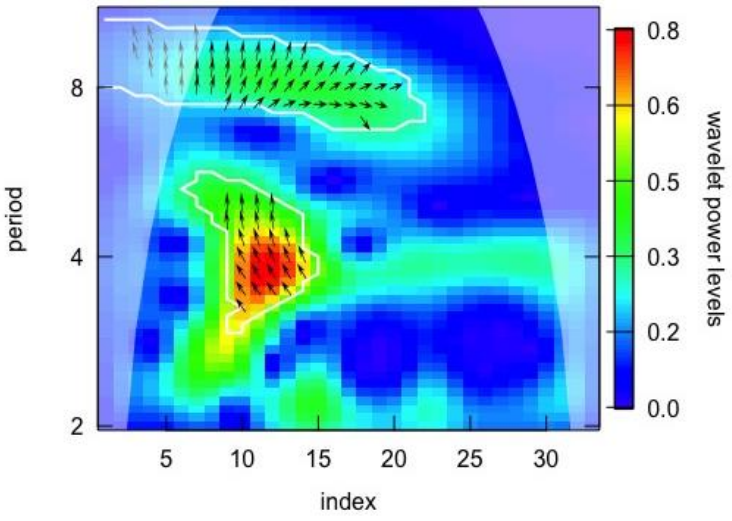

*Figure **26** Cross-wavelet power between smoothed SPG annual anomalies throughout the SPG basin between and sea ice area fraction annual anomalies throughout the Denmark strait between 1980 and 2012 in the NAX simulation. The color bar indicates the relevance, red colors mean higher relevant period. The direction of the arrows indicates the lead – lag relationship between the variables, in this case density leads.*

between the sea ice fraction and the SPG variability when SPG lags with a very strong power (Figure 26), especially between 1990 and 1995.

4.3- Mechanisms of SPG variability: comparative analysis of lead – lag correlation and regression in *GI3*

The last transient simulation GI3 has different characteristics from the *NA* simulation: the coupled area is in Arctic region and it covers a longer time period (85 years). Comparison with the evolution of the driving variables in the *NA* simulations are difficult to interpret due to the different periods of time considered, even though it is possible to notice some agreement when looking at the overlapping period between 1980 and 2000.

Starting from the SST relation with SPG variability, the *GI3* simulation shows a long lasting positive annual anomaly starting around 1960 and lasting until the end of the series (Figure 27).

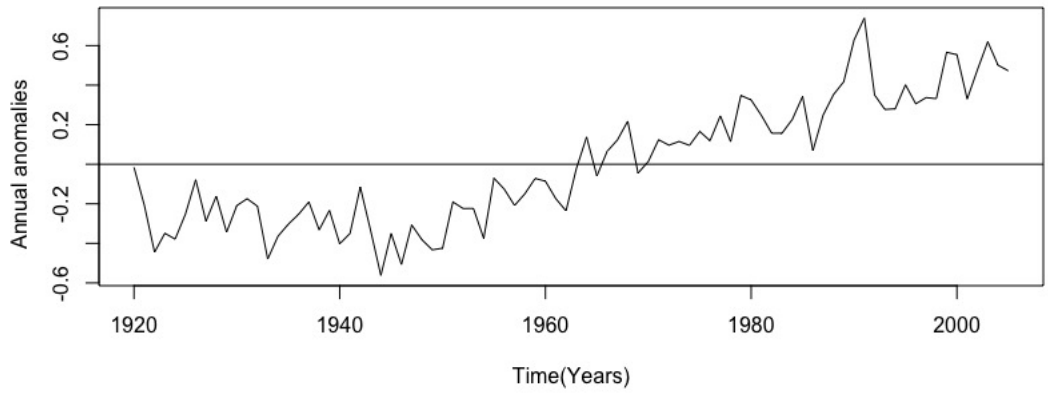

*Figure **27** Smoothed annual anomalies of variable SST of GI3 simulation throughout the SPG basin calculated between 1920 and 2005*

The onset of the long-term increase (not shown) can be the Arctic warming event around 1940, and its continuation a result of global warming. After the 1940s, we can notice a slow decrease in the SPG (Figure 5a) that can confirm the link between these two variables, which was consistently found in the *NA* simulations as well. The lead-lag correlation analysis shows strange spatial patterns at different lags in the light of the same analysis on the *NA* simulations (Figure 28): the whole basin has a strong negative correlation either SPG is leading or lagging, on annual or sub-seasonal period with just a small positive correlated area in the eastern part of the basin. A possible explanation of this result is the strong long-term trend detected in this simulation, which might dominate the correlation analysis. On the contrary the regression analysis is closer to what was obtained in the *NA* simulations,

showing a negative area in the southern part of the basin, probably suggestive of a link with the Gulf stream or the subtropical gyre, and positive areas in the eastern part of the basin (Figure 29).

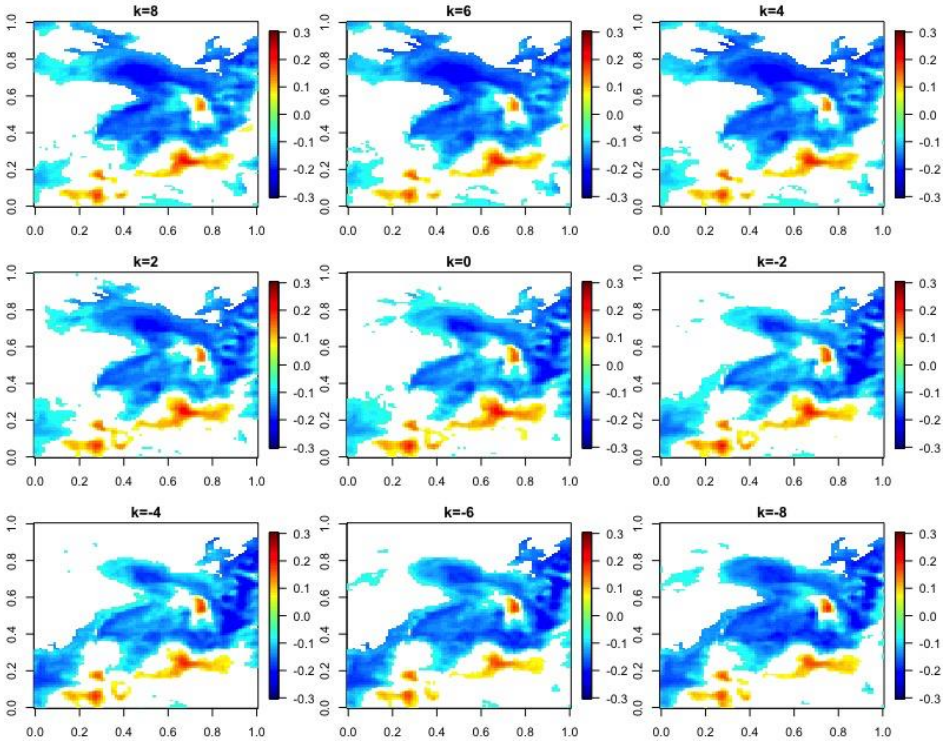

*Figure **28** Sub-seasonal changes in the short-term lead-lag correlation between SPG variability and SST in the subpolar basin for GI3 simulation between 1920 and 2005. Only significant correlated areas above the 95% confidence level are shown. Positive values of lag k mean that SPG lags while the negative values of the lag k mean that the SPG leads changes in the SST.*

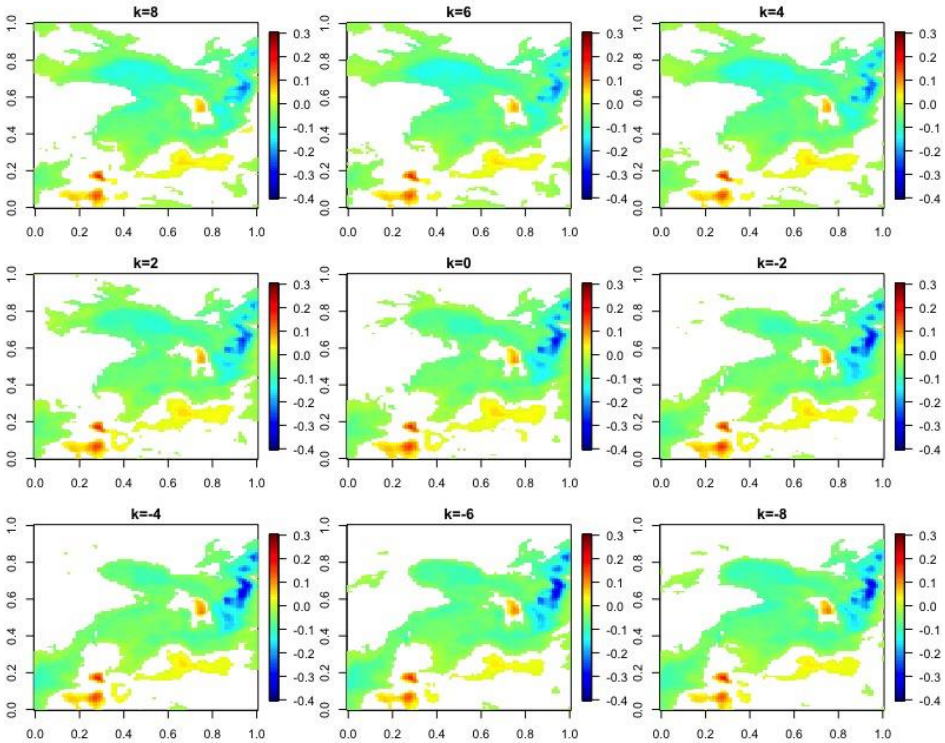

*Figure **29** Sub-seasonal changes in the short-term lead-lag regression between SPG variability and SST in the subpolar basin for GI3 simulation between 1920 and 2005. Only significant correlated areas above the 95% confidence level are shown. Positive values of lag k mean that SPG lags while the negative values of the lag k mean that the SPG leads changes in the SST.*

Accordingly, also SSS shows and initial period between 1920 and 1950, followed by an increase as detected by the positive annual anomalies between 1960 and late 1990s (Figure 30).

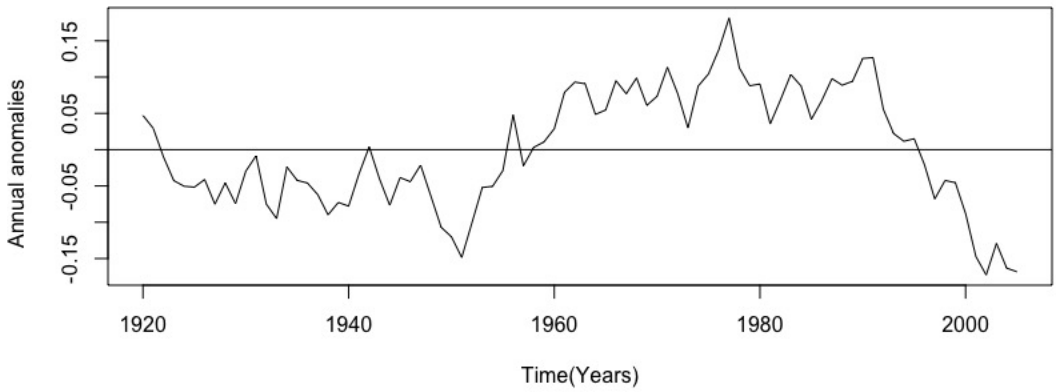

*Figure **30** Smoothed annual anomalies of variable SSS of GI3 simulation throughout the SPG basin calculated between 1920 and 2005*

This is rather coherent with the *NA* simulations that are characterized by a decreasing trend after 1980, which is also found here, even though in *GI3* the trend is decreasing with a low interannual variability until 2000, while in the *NA* simulations this trend has more interannual variability (not shown). The lead-lag correlation analysis agrees with the *NA* simulation in underlying the differences in the relationship, especially for annual changes, between the two opposite side of the basin: eastern within the Denmark Strait and western within the Labrador Sea (Figure 31). Particularly, when the SPG lags we can notice a positive correlation in Denmark strait and a negative correlation within the Labrador Sea. The regression analysis is

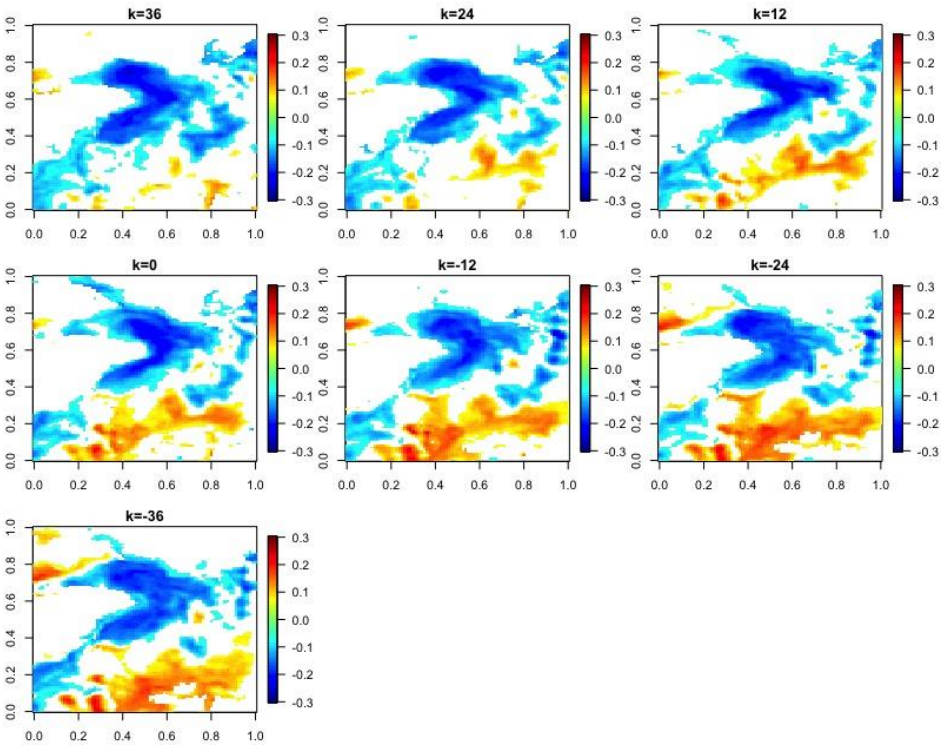

*Figure **31** Yearly changes in the short-term lead-lag correlation between SPG variability and SSS in the subpolar basin for GI3 simulation between 1920 and 2005. Only significant correlated areas above the 95% confidence level are shown. Positive values of lag k mean that SPG lags while the negative values of the lag k mean that the SPG leads changes in the SSS.*

consistent with the results of the *NA* simulation, in showing a negative correlated area in the southern part of the basin that suggests a negative interaction between the subpolar gyre and the subtropical gyre (Figure 32).

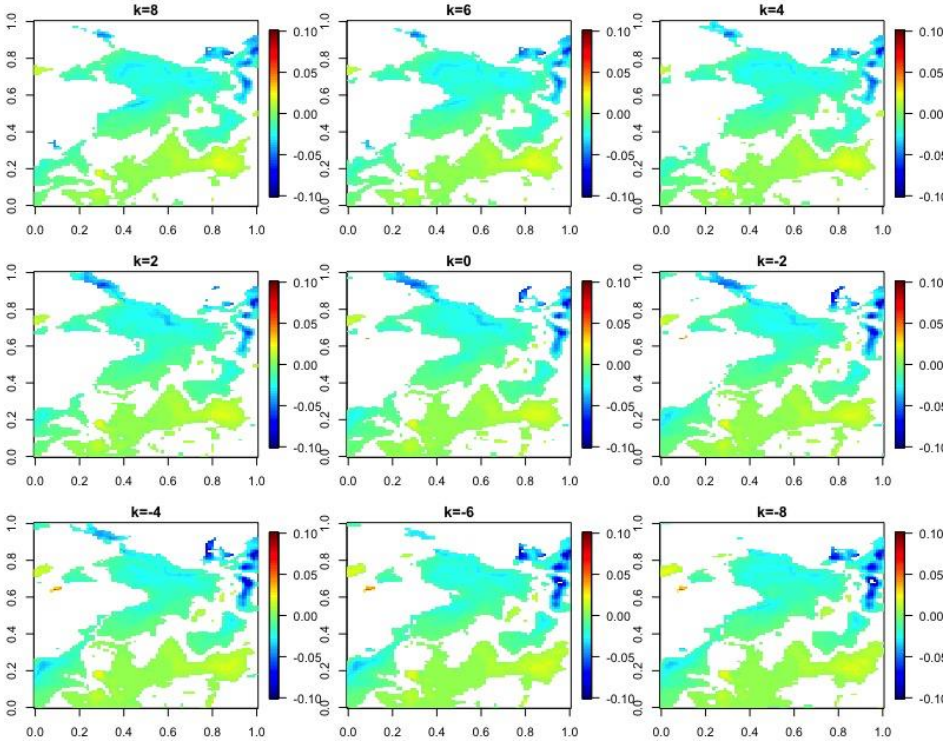

*Figure **32** Sub-seasonal changes in the short-term lead-lag regression between SPG variability and SSS in the subpolar basin for GI3 simulation between 1920 and 2005. Only significant correlated areas above the 95% confidence level are shown. Positive values of lag k mean that SPG lags while the negative values of the lag k mean that the SPG leads changes in the SSS.*

The long-term evolution of TFWF indicates a large interannual variability throughout the whole period, further proven by the alternation of positive and negative anomalies (Figure 33), with signs of predominance of positive anomalies at the end of the XX century. Likewise, in this case more apparent linkages between SPG variability and TFWF would have emerged with time series related to smaller regions, such as the Labrador Sea and the Denmark Strait.

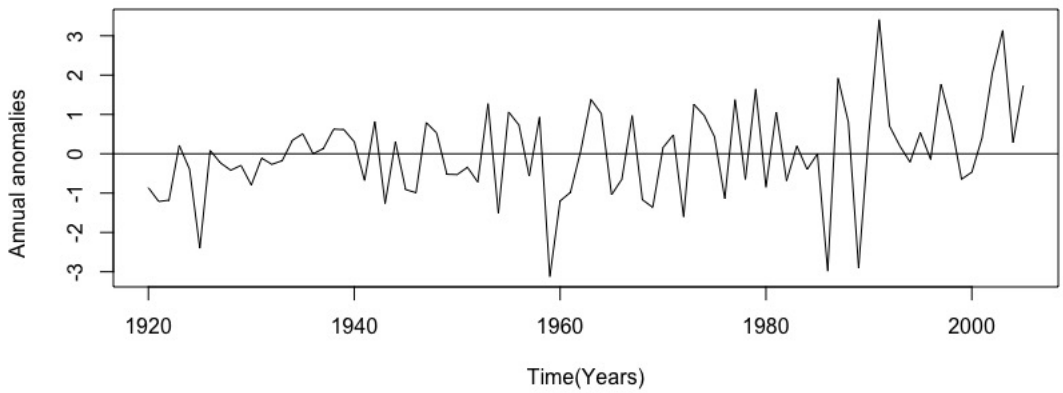

*Figure **33** Smoothed annual anomalies of variable TFWF of GI3 simulation throughout the SPG basin calculated between 1920 and 2005*

Nevertheless, the lead-lag correlation analysis confirms the results of the *NA* simulations especially the positive correlation that exists in the Denmark strait (Figure 34, not very clear but Denmark strait is the bottom left part of the figure).

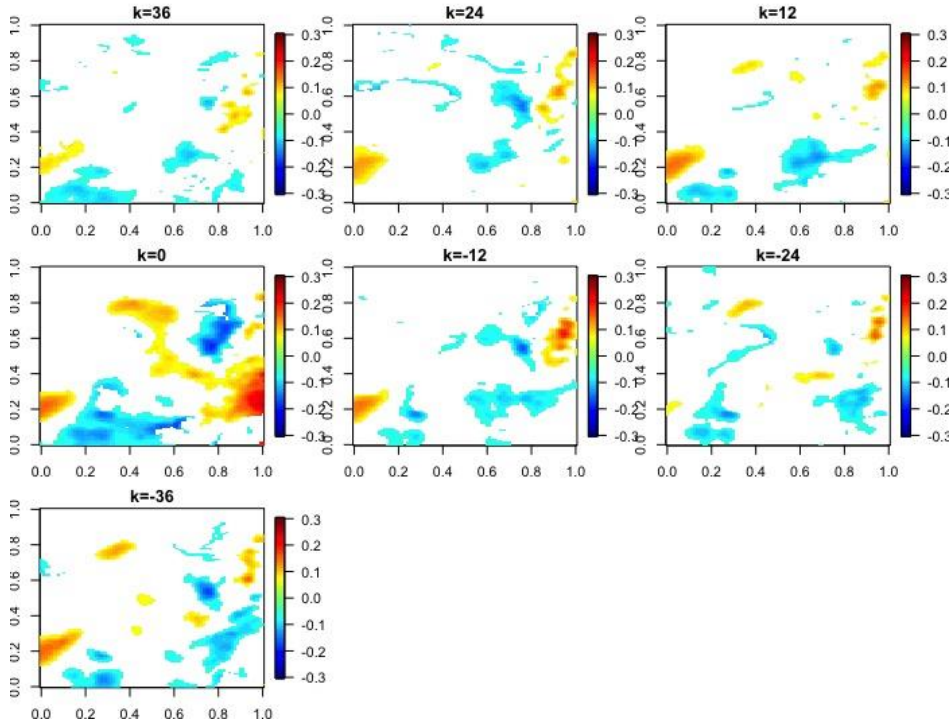

*Figure **34** Yearly changes in the short-term lead-lag correlation between SPG variability and TFWF in the subpolar basin for GI3 simulation between 1920 and 2005. Only significant correlated areas above the 95% confidence level are shown. Positive values of lag k mean that SPG lags while the negative values of the lag k mean that the SPG leads changes in the TFWF*

Finally, the long-term evolution of the Sea ice area fraction in the Denmark Strait characterized by large interannual variations (as in the *NA* simulations) especially between 1930 and 1940, followed a period characterized by positive anomalies. From 1960 to the end of the series, the variables show a decreasing trend, characterized by negative annual anomalies especially around 2000.

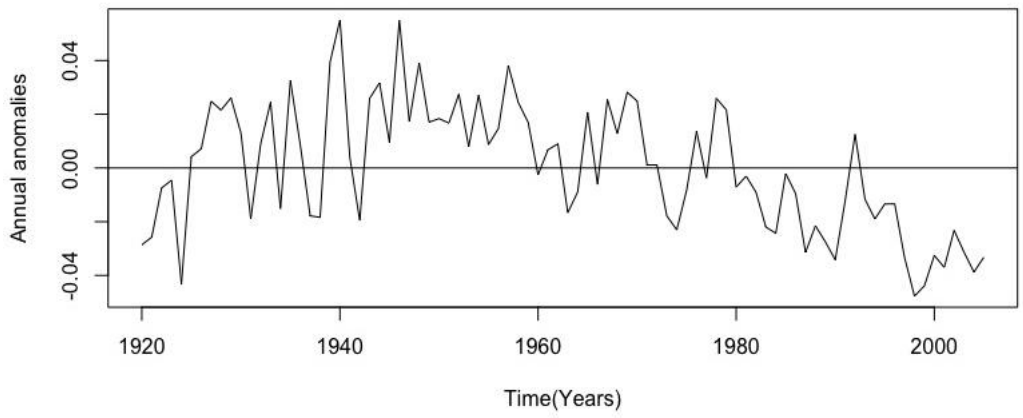

*Figure **35** Smoothed annual anomalies of variable sea ice fraction of GI3 simulation throughout the Denmark Strait calculated between 1920 and 2005*

The results of the wavelet analysis results exhibit few interesting patterns. There is just a higher power period around 1940, where the two series are in phase with SPG lagging to changes in the sea ice are fraction in Denmark Strait (Figure 36).

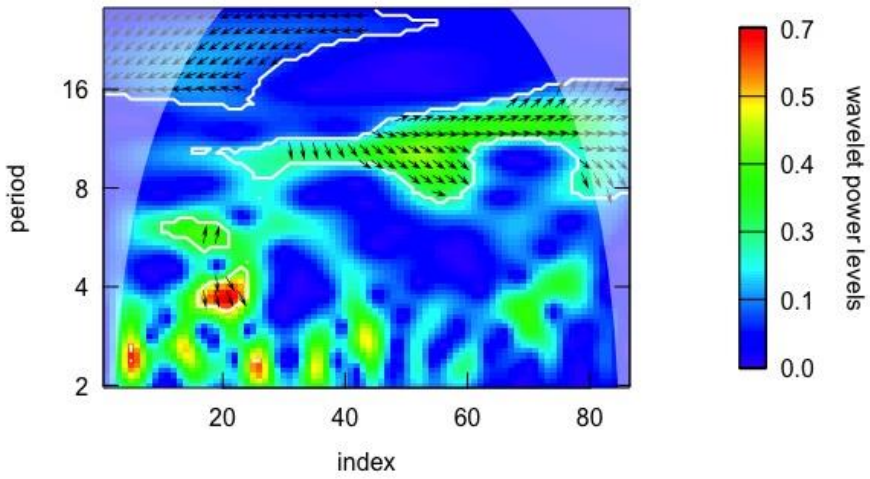

*Figure **36** Cross-wavelet power between smoothed SPG annual anomalies throughout the SPG basin between and sea ice area fraction annual anomalies throughout the Denmark strait between 1920 and 2005 in the GI3 simulation. The color bar indicates the relevance, red colors mean higher relevant period. The direction of the arrows indicates the lead – lag relationship between the variables, in this case SPG lags.*

4.4- The relation between SPG, meridional heat transport and AMOC

In this section I investigate the linkages between the AMOC and the SPG in relation with the meridional oceanic heat transport at the surface and AMOC calculated at different depth: surface (0m), 524m and 1024m depth in the North Atlantic Ocean. The output from all the four simulations is considered in the analysis.

For the heat transport, the three NA simulations show a similar, almost linear trend and a similar range and evolution of the annual anomaly (Figure 37). *Gi3* shows more variability compared to the NA simulations, but it agrees with them on the general decreasing trend (Figure 38). The correlation coefficient between SPG and the meridional heat transport for NAS and *NAT* was not statistically significant. *NAX* simulation shows a low positive correlation coefficient (Spearman correlation coefficient 0.16, $p<0.05$), while *GI3* show a higher positive correlated value (Spearman correlation coefficient 0.52, $p<0.05$). Previous studies (e.g. Moreno-Chamarro et al., 2016) have suggested that at subpolar latitudes the meridional oceanic heat transport is mainly driven by the SPG, and a weaker state of the SPG is associated with a decrease in the meridional heat transport.

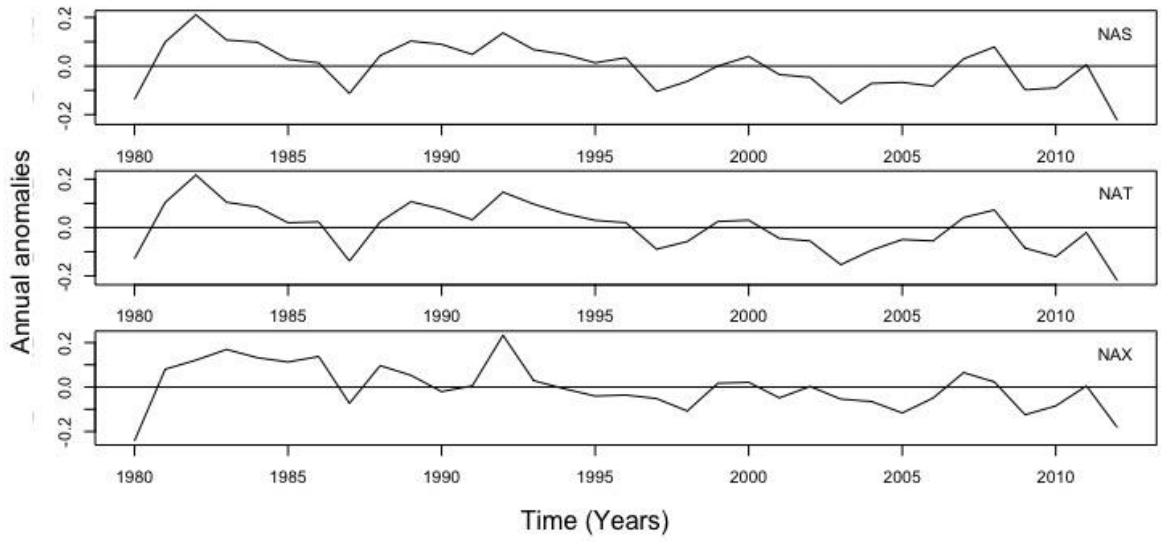

*Figure **37** Smoothed annual anomalies of variable meridional heat transport of NA simulations throughout the North Atlantic Ocean calculated between 1980 and 2012*

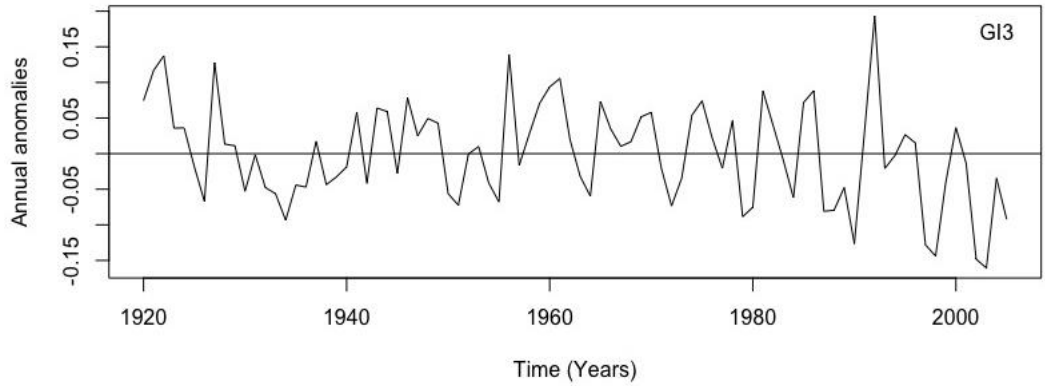

*Figure **38** Smoothed annual anomalies of variable meridional heat transport of GI3 simulation throughout the North Atlantic Ocean calculated between 1920 and 2005*

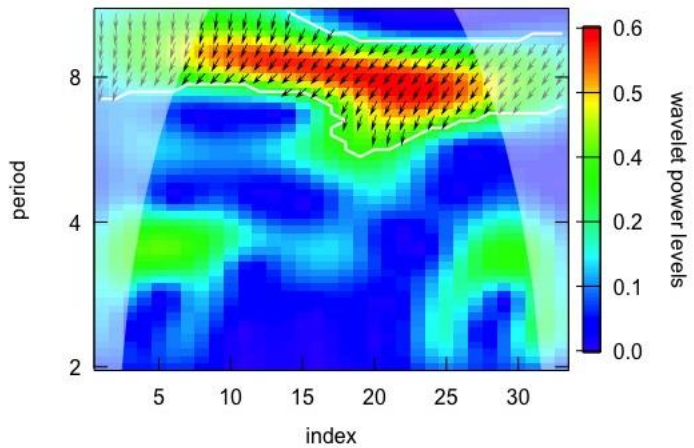

From the wavelet analysis we can see a rather robust antiphase relation at near-decadal timescales between SPG and meridional ocean heat transport in the *NAS* (Figure 39) and *NAT* simulations, which holds especially after 1990.

*Figure **39** Cross-wavelet power between smoothed SPG annual anomalies and meridional heat transport annual anomalies throughout the North Atlantic Ocean between 1980 and 2012 in the NAS simulation. The color bar indicates the relevance, red colors mean higher relevant period. The direction of the arrows indicates the lead – lag relationship between the variables, in this case SPG leads.*

In *NAX* and *GI3,* the results are of difficult interpretation since there is a superposition of different phases, in different frequencies and it is difficult to exactly affirm which variable is leading and lagging.

The relation between the AMOC and the SPG, at the surface agrees within the *NA* simulations. The long-term evolution is constant al the surface level (Figure 40) but looking at depths of 524 m and 1024 m the simulations show a decreasing trend that starts around 2000 (Figures 41 and 42). The same weakening is also found in the SPG time series for *NAS* and *NAT*, where it seems to start a bit earlier (compare with Figure 4), while for *NAX* where at constant (slight increasing) values of the SPG is associated a decrease in the value of the AMOC (compare with Figure 4).

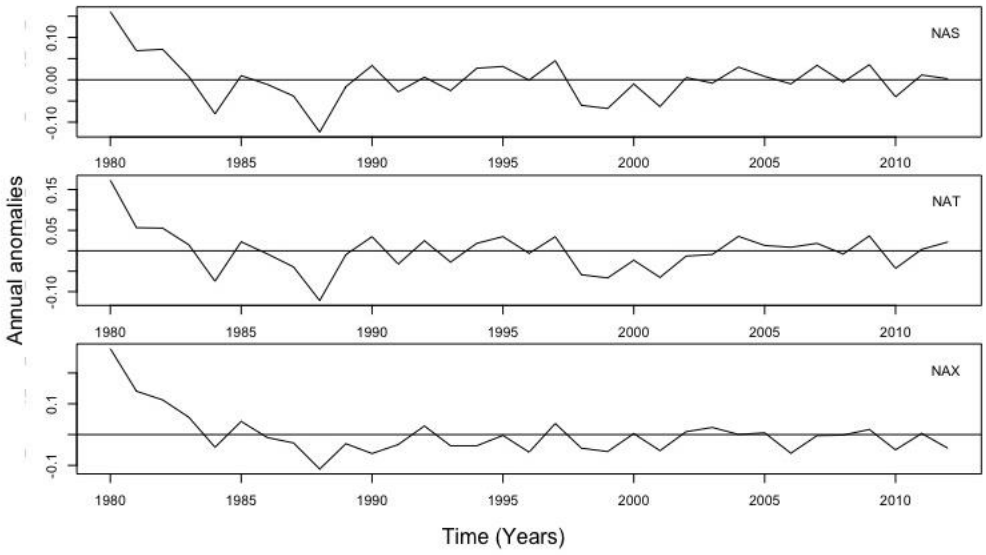

*Figure **40** Smoothed annual anomalies of AMOC of NA simulations throughout the North Atlantic Ocean calculated between 1980 and 2012 at the surface level (0 m)*

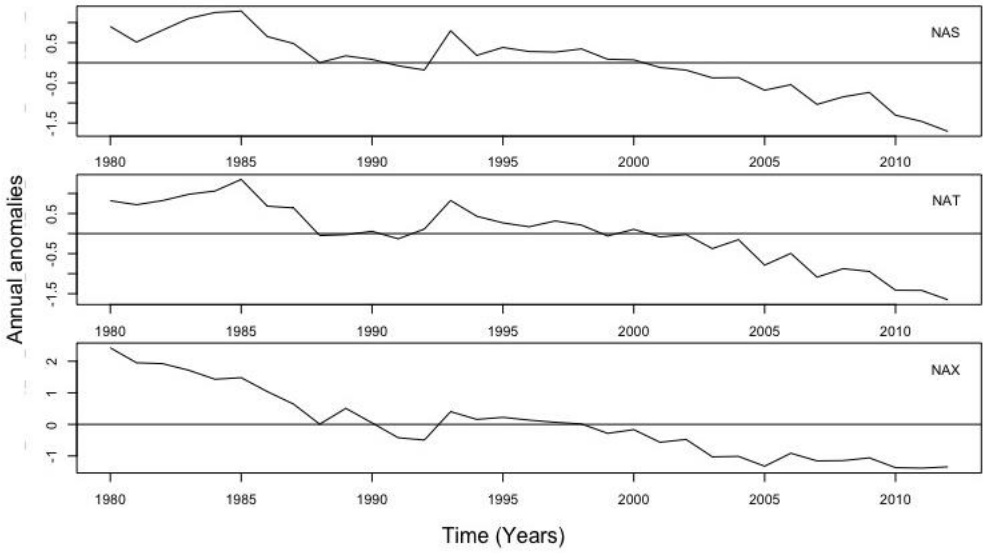

*Figure **41** Smoothed annual anomalies of AMOC of NA simulations throughout the North Atlantic Ocean calculated between 1980 and 2012 at 524m depth*

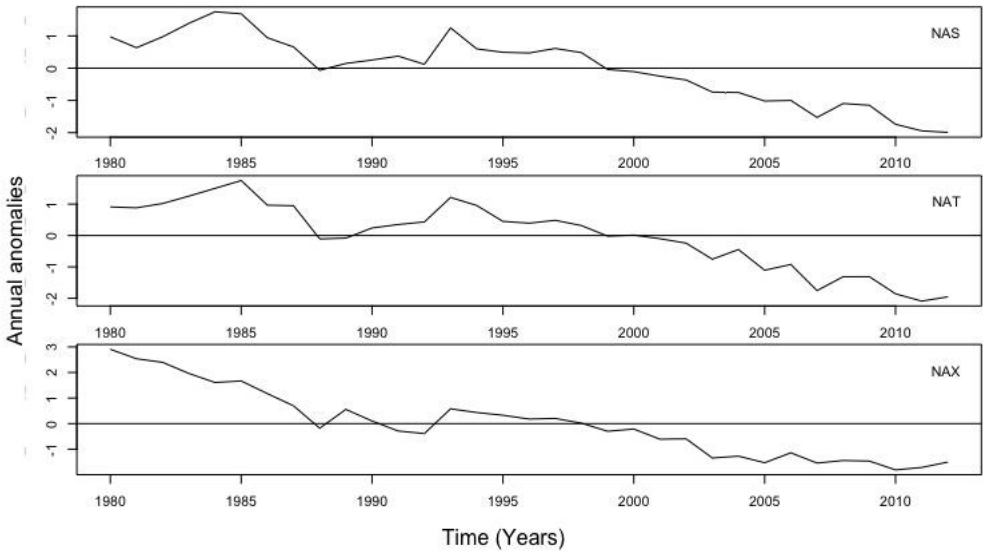

*Figure **42** Smoothed annual anomalies of AMOC of NA simulations throughout the North Atlantic Ocean calculated between 1980 and 2012 at 1024m depth*

Since the most significant values for AMOC changes are at a depth of 1000m, the correlation coefficients and wavelet analysis has been performed between the SPG time series and AMOC time series calculate at that depth. Specifically, the correlation coefficients calculated between the AMOC and the SPG time series at 1024 are positive for *NAS* (Spearman correlation coefficient 0.35, $p<0.05$) and *NAT* (Spearman correlation coefficient 0.34, $p<0.05$), while the *NAX* simulation the correlation between AMOC and SPG time series was not statistically significant. From the wavelet analysis we can see, in the *NAX* simulation, a first robust antiphase relation around 1990 where the significance area for the power analysis and phase analysis fall together and a rather weak antiphase relation at near-decadal timescales between SPG and AMOC which holds especially after 1995 in both cases with SPG leading (Figure 43). In *NAS* and *NAT* the results are of difficult interpretation since there is any overlapping between the phase and wavelet power analyses.

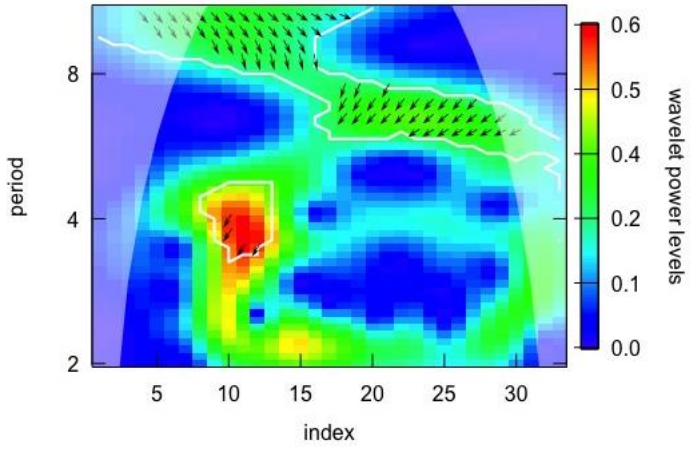

*Figure **43** Cross-wavelet power between smoothed SPG annual anomalies AMOC annual anomalies throughout the North Atlantic Ocean between 1980 and 2012 in the NAX simulation. The color bar indicates the relevance, red colors mean higher relevant period. The direction of the arrows indicates the lead – lag relationship between the variables, in this case SPG leads after 1990.*

Concluding, in the simulation GI3, accordingly to the *NA* simulations show a decreasing trend especially at the end of the 1990s (Figure 44). This simulation confirms the positive correlation coefficient in agreement with *NAS* and *NAT* (Spearman correlation coefficient 0.26, $p<0.05$).

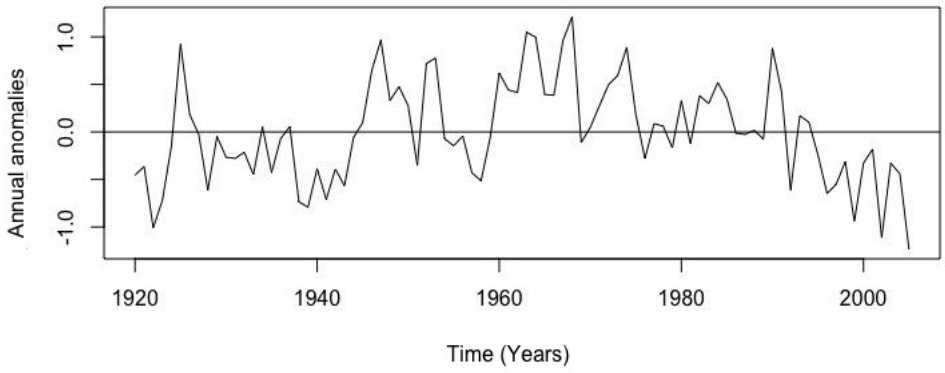

*Figure **44** Smoothed annual anomalies of AMOC of GI3 simulations throughout the North Atlantic Ocean calculated between 1920 and 2005 at 1020m depth*

The wavelet analysis (Figure 45) show a weak antiphase between SPG and AMOC around 1950 with SPG leading and a followed by another weak antiphase between 1960 and 1980 with SPG lagging.

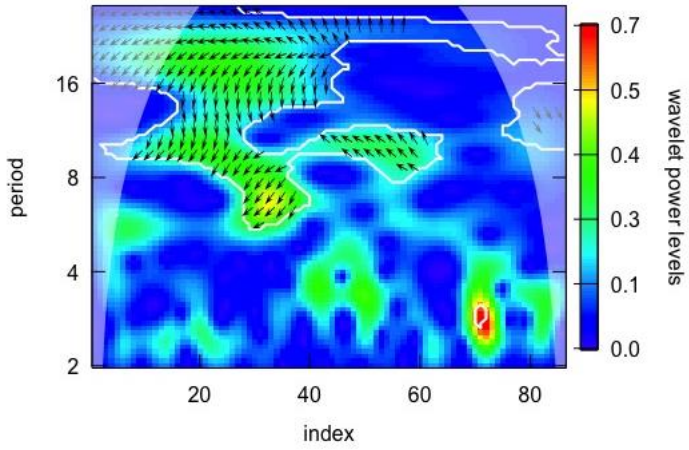

*Figure **45** Cross-wavelet power between smoothed SPG annual anomalies AMOC annual anomalies throughout the North Atlantic Ocean between 1920 and 2005 in the GI3 simulation. The color bar indicates the relevance, red colors mean higher relevant period. The direction of the arrows indicates the lead – lag relationship between the variables, in this case SPG leads around 1950 and lags between 1960 and 1980.*

SECTION D: DISCUSSION AND CONCLUSION

5.1- The nature of the simulated SPG variability

The Na simulations show marked differences regarding various aspects of the temporal evolution of the SPG strength. A first aspect in this sense is the long-term tendency, which develops similarly in *NAT* and *NAS*, whose agreement is further supported by a high correlation coefficient. Both simulations exhibit an initial increasing trend, here defined as the slowly varying component determining the time series level after the seasonal components have been removed, with a peak in the values around 1995, which is successively followed by a decline. Previous studies have confirmed a decreasing in the SPG strength, for instance a weakening of the SPG between 1992 and 1997 has been documented by both direct observations (e.g. Häkkinen and Rhines 2004) or by other model studies (e.g. Böning *et al*., 2006). These results agree in suggesting a general weakening of the SPG in this time span notwithstanding the index has been calculated differently within the studies (e.g., using the Sea Surface Height). This weakening has been associated with a warming of the SPG basin late in the mid 1990s (e.g. Robson et al., 2012), possible causes of the which, according to Häkkinen et al., 2004, are linked to changes in the ocean circulation and, again, changes in the NAO phase (specifically its strong positive phase). On the contrary, the NAX simulation exhibits a different evolution of SPG variability with time compared to NAT and NAS. Specifically, this simulation does not show the increasing and, then, decreasing trends, nor the pick in 1995. On the contrary, its long-term evolution is characterized by an almost constant trend except for between 1990 and 1995. However, all the *NA* simulations show some interannual variability, while no prominent decadal variability emerges within the investigated time period. The fourth simulation, *GI3*, shows both interannual and decadal variability (particularly visible between 1930-1940). The discrepancies between *GI3* and the *NA* simulation arise not only in the long-term evolution but more interestingly in the range of the climatological means that in *GI3* is lower than in *NAs.*

5.2- The relation between SPG variability and the driving variables

Lead-lag correlation and linear regression together with wavelet analyses have been performed to describe the relation between the SPG variability and the selected driving variables SST, SSS, density, TWFW and sea ice fraction area in the Denmark Strait. Accordingly, NAT and NAS manifest the same relationships within the results but also NAX show an overall consistent behavior. The three *NA* simulations show, even though with some differences, the differences in the ocean surface

properties between the eastern and western SPG basin and within the gyre's center and its boundaries. This is particularly clear for SSS and density when the SPG leads ($k < 0$). A stronger state of the SPG transports more high-salinity waters from the Tropical Atlantic via the Gulf Stream (thus a positive correlation between the variables especially in the eastern part of the basin). This will produce an increase of the density gradient between the gyre center and its exterior boundaries (e.g., Born and Leverman, 2007). The relation between the SPG and SST changes are less consistent, hence of more difficult interpretation. SSTs are strongly related to heat surface fluxes and heat transport in the SPG basin. A weaker SPG, indeed, is linked to reduced recirculation within the subpolar North Atlantic, hence it transports less heat westward and the SST in the Labrador Sea cools producing an increase in the upper ocean density that can contribute to strengthen of the SPG. Secondly, cooling or warming of the sea surface temperatures in the different parts of the basin are strongly related and determined by increasing or decreasing in the fresh water export from the Arctic and Nordic Seas (e.g. Born *et al., 2010*). An increase in the freshwater input to the SPG basin, especially due to the solid component of the total fresh water export from the Arctic, influences vertical mixing and deep water convection as the sea ice remains concentrated at the surface at acts toward hampering surface energy fluxes (e.g. Born *et al., 2010*). Then, the SPG strength is influenced too: sea ice exported from the Arctic is successively transported southward, where warmer water from the Tropical Atlantic melts it progressively, thus decreasing SSSs of the upper Atlantic Ocean, eventually yielding a SPG weakening (e.g. Moreno-Chamarro *et al.,* 2016). The results for all simulations reveal a negative correlation in the Labrador region with SSTs when the SPG leads, while contrasting results emerge when the SPG lags as both cooling or warming emerges at the sea surface in different simulations. Interesting results are shown for the TFWF import that emerges to be negatively correlated with SPG variability when the SPG lags, i.e., as said before a higher quantity of fresh water export especially through the Denmark Strait leads to a weakening of the SPG. *GI3* simulation cannot clearly resolve the interaction between SST, SSS and density and TFWF as well as the *NA* simulations. This can be a consequence of the non-stationarity of the relationship between SPG and the driving variables visible on longer time scales. In this case the general relation between the driving variables and SPG variability agrees between the *NA* simulation, even though still differences persist especially with the NAX simulation.

5.3- Differences among the simulations

As already explained in the previous sections the *NA* simulations provide different results especially in the general long-term tendency of the SPG. The consistency between the SPG evolutions in the NAS and NAT simulations suggest that the atmospheric forcing of the ocean circulation in the region outside the coupled domain, such as in the tropical Atlantic region, dominates over the SPG variability induced by processes in the coupled region, such as the freshwater export from the Arctic. On the contrary, the different evolution of the NAX simulation suggests that NAS and NAT may miss small-scale phenomena in the coupled region that substantially contribute to SPG variability. However, the present Thesis cannot provide strong evidences and conclusions, neither about the internal climate variability due to the "random" variability that spontaneously arise due to the chaotic and nonlinear character of the system (highlighted by differences among the *NA* simulations), nor it can reveal robust effects of external forcing (highlighted by consistent behavior). In fact, in the light of the results achieved here, three simulations are not enough to clarify the SPG variability accounting for the differences in the employed REMO setups. However, the *NA* simulations as well as *GI3* show an overall good agreement when looking at the relation between SPG variability, AMOC and heat transport (further in section 5.4). This suggests that changes in the AMOC can be led by changes in the SPG strength alone, especially due to changes in the Labrador Sea deep water convection (e.g. Moreno-Chamarro *et al.*, 2016) and not necessarily due to changes in the NAO phase.

5.4- The interaction between the SPG variability, AMOC and heat transport

The interaction between the SPG variability and AMOC is well resolved in all the transient simulations (*NA*S and *GI3*). The simulations agree in showing a decreasing trend in the AMOC, which is particularly visible in the mass transport at 1024 m depth. This suggests that the *boundary effect* due to the imposed TFWF changes in the SPG basin are enough to induce consistent changes in the AMOC in the different setups of ROM. Accordingly, changes in the dense water formation within the subpolar basin in the DWBC, that is the lower branch of the AMOC, and in the deep water convection in the Labrador Sea, that is one of the key processes feeding the AMOC, contribute to changes the AMOC transport (e.g. Böning *et al.,* 2006). These evidences support the idea that the SPG alone is capable of modulating the AMOC notwithstanding the occurrence of an anomalous NAO phase. Finally, the meridional heat transport is characterized by an almost constant trend. In subpolar latitude the meridional heat transport is principally driven by the SPG (e.g. Moreno-Chamarro *et al.,* 2016) where weaker state of the SPG produce a reduction in the heat transport.

5.5- Conclusion and outlooks

I investigate interannual to decadal changes of the SPG variability, underling the differences between three transient climate model simulations with a different atmospheric resolution (*NA)*. The idea was that differences among the simulations would reveal that changes in the SPG variability are associated to internal climate variability, while consistent behavior would reveal the predominance of the effect of external forces. I further integrate this analysis with a fourth simulation where the ocean-atmosphere coupling is activated in the SPG/Arctic instead of in the Tropical Atlantic, in order to study the role of different contributions to SPG dynamics. Secondly, since SPG variability has been mainly associated with buoyancy fluxes differences, I evaluate the relation between the SPG variability and SST, SSS, density, TFWF within the SPG basin and sea ice dynamics as sea ice fraction area throughout the Denmark Strait. I also explore the relation between the SPG, AMOC and meridional oceanic heat transport. These analyses are supported by time series analysis, lead-lag correlation and linear regression analysis, and wavelet analysis. Results indicate that:

1. The interannual variability of the SPG characterizes all the *NA* simulations and the *GI3* simulations that also shows a period between 1930-1940 of prominent decadal variability. Differences among the *NA* simulations indicate that the two simulations with lower atmospheric resolution do not resolve small scale atmospheric processes that may be relevant for SPG variability. By these differences, nevertheless, it is not possible to conclude about the dependency of SPG variability on external forcing.
2. The relation between the driving variables and the SPG strength are rather consistent within the *NA* simulations, even though some remarkable differences persist. The results show differences among the eastern and western part of the basin and between the gyre's center and its boundaries especially for SSS, density and TFWF, while not so clearly for SST. *GI3* show different relations compared to the NA simulations, suggesting that either a different mechanism dominates in this simulation or that different mechanisms contribute to SPG variability during the longer simulated period (85 years compared to the 32 of the *NA* simulations). Of special relevance is the lack of signals related to the interaction between SPG variability and TFWF, which was expected to be highlighted in this simulation via boundary forcing.
3. The relation between the SPG variability, AMOC and meridional heat transport agrees within the four transient simulations in showing the same long-lasting decrease. These results

support the host of recent studies suggesting that the SPG has the capability to modulate alone the AMOC.

The achieved results provide a basis for further investigations. First, a larger number of simulations is needed in order to better identify the role of the different atmospheric resolutions on the results. The present study, moreover, did not consider superficial heat fluxes and exchanges between the ocean and the atmosphere even though these fluxes are a strong component for SPG variability and strength. These fluxes were not used here due to difficulties in the availability of the data. The follow-up research comprises the evaluation of future scenarios especially in relation with anthropogenic climate changes, as this is thought to be able to produce even great impacts on the North Atlantic and thus, possibly, on the SPG. A better and deeper description of the differences among the eastern and western part of the SPG basin in order to better characterize the anomalous buoyancy fluxes that lead SPG variability. As a concluding remark, progress in our understanding of the SPG variability requires its improved characterization via instrumental observations. Only with data available to compare different climate models results, we can build knowledge about the functioning of the climate system.

AKWNOLEDGMENTS: I'm particularly grateful to Dmitry Sein from Alfred Wegener Institute for Polar and Marine Research (Germany) for providing me the ROM simulations and access to his new state-of-the-art model.

REFERENCES

Aagaard, K., & Carmack, E. C., 1989. *The role of sea ice and other fresh water in the Arctic circulation*. Journal of Geophysical Research: Oceans, 94(C10), 14485-14498.

Aguiar-Conraria L., and Soares M.J., 2011. *The Continuous Wavelet Transform: A Primer*. NIPE Working Paper Series 16/2011.

Arakawa, A., Lamb V. R., 1977. *Computational design of the basic dynamical processes of the UCLA general circulation model*. Methods Comput. Phys., 17, 173–265.

Bacon, S., 2002. *The dense overflows from the Nordic Seas into the deep North Atlantic*. Presented at: ICES Symposium 100 Years of Science Under ICES, Helsinki, Finland, 1–4 August 2000 215, 148–155.

Böning, C. W., M. Scheinert, J. Dengg, A. Biastoch, and A. Funk, 2006. *Decadal variability of subpolar gyre transport and its reverberation in the North Atlantic overturning*. Geophys. Res. Lett., 33, L21S01.

Born, A., & Mignot, J., 2012. *Dynamics of decadal variability in the Atlantic subpolar gyre: a stochastically forced oscillator*. Climate dynamics, 39(1-2), 461-474.

Born, A., Stocker T. F., 2014. *Two stable equilibria of the Atlantic subpolar gyre*, J. Phys. Oceanogr., 44(1), 246–264.

Brauch, J. P., & Gerdes, R., 2005. *Response of the northern North Atlantic and Arctic oceans to a sudden change of the North Atlantic Oscillation*. Journal of Geophysical Research: Oceans, 110(C11).

Broecker, W. S., 1997. *Thermohaline circulation, the Achilles heel of our climate system: Will man-made CO2 upset the current balance?*. Science, 278(5343), 1582-1588.

Delworth, T., Manabe, S., & Stouffer, R. J., 1993. *Interdecadal variations of the thermohaline circulation in a coupled ocean-atmosphere model*. Journal of Climate, 6(11), 1993-2011.

Delworth, T. & Mann, M. Climate Dynamics, 2000. *Observed and simulated multidecadal variability in the Northern Hemisphere*. Clim. Dyn., 16, 9, 661-667.

Deshayes J., Frankignoul C., 2008. *Simulated variability of the cir- ulation in the North Atlantic from 1953 to 2003*. J. Clim. 21(19), 4919–4933.

Dickson, R., Brown, J., 1994. *The production of North-Atlantic deep waters — sources, rates, and pathways*. J. Geophys. Res. Oceans 99 (C6), 12319–12341. Miniconference on Observation and Modeling of North Atlantic Deep Water Formation and its Variability. Columbia University, Lamont Doherty Earth Observations, Pal- isades, NY (November).

Dickson, R., Rudels, B., Dye, S., Karcher, M., Meincke, J., Yashayaev, I., 2007. *Current estimates of freshwater flux through Arctic and subarctic seas*. Prog. Oceanogr. 73 (3–4), 210–230.

Dunne, J.P., J.G. John, E. Shevliakova, R.J. Stouffer, J.P. Krasting, S.L. Malyshev, P.C. Milly, L.T. Sentman, A.J. Adcroft, W. Cooke, K.A. Dunne, S.M. Griffies, R.W. Hallberg, M.J. Harrison, H. Levy, A.T. Wittenberg, P.J. Phillips, and N. Zadeh, 2013: GFDL's ESM2 Global Coupled Climate–Carbon Earth System Models. Part II: Carbon System Formulation and Baseline Simulation Characteristics. J. Climate, 26, 2247–2267.

Eden, C., Willebrand, J., 2001. *Mechanism of interannual to decadal variability of the North Atlantic circulation*. J. Clim. 14 (10), 2266–2280.

Flato, G. M. 2011. *Earth system models: an overview*. WIREs Clim Change, 2: 783-800. doi:10.1002/wcc.148.

Flato G., J. Marotzke, B. Abiodun, Pascale Braconnot, S.C. Chou, et al.. Evaluation of climate models. Climate Change 2013 – The Physical Science Basis: Working Group I Contribution to the Fifth Assessment Report of the Intergovernmental Panel on Climate Change, Cambridge University Press, pp.741-866, 2013, 9781107415324.

Furevik, T., Bentsen, M., Drange, H., Johannessen, J. A., & Korablev, A., 2002. Temporal and spatial variability of the sea surface salinity in the Nordic Seas. Journal of Geophysical Research: Oceans, 107(C12), SRF-10.
García-Ibanez M.I., Pardo P.C., Carracedo L. I., Mercier H., Lherminier P., Rios F.A., Pérez F.F., 2015. *Structure, transports and transformations of the water masses in the Atlantic Subpolar Gyre.* Progress in Oceanography, 135, pp 18-36.

Goosse H., P.Y. Barriat, W. Lefebvre, M.F. Loutre and V. Zunz, 2010. *Introduction to climate dynamics and climate modelling*. pp 59 – 86.

Hagemann, S., and Dumenil L., 1998. *A parameterization of the lateral waterflow for the global scale*, Clim. Dyn., 14, 17–31.

Hagemann, S., and Dumenil L. Gates, 2001. *Validation of the hydrological cycle of ECMWF and NCEP reanalyses using the MPI hydrological discharge model*, J. Geophys. Res., 106, 1503–1510.

Hakkinen, S., & Rhines, P. B., 2009. *Shifting surface currents in the northern North Atlantic Ocean*. Journal of Geophysical Research: Oceans, 114(C4).

Haine, T., Böning, C., Brandt, P., Fischer, J., Funk, A., Kieke, D., Kvaleberg, E., Rhein, M., Visbeck, M., 2008. *North Atlantic deep water transformation in the Labrador Sea, re- circulation through the subpolar gyre, and discharge to the subtropics*. Defining the Role of the Northern Seas in Climate. Arctic Subarctic Ocean Fluxes. Springer, Netherlands, 653–701.

Hátún H., Sandø A. B., Drange H., Hansen B., Valdimarsson H., 2005. *Influence of the Atlantic subpolar gyre on the thermohaline cir-culation*. Science 309(5742), 1841–1844.

Hibler, W. D., 1979. *A dynamic thermodynamic sea ice model*. J. Phys. Oceanogr., 9, 815–846.

Higginson, S., Thompson, K.R., Huang, J., Veronneau, M., Wright, D.G., 2011. *The mean surface circulation of the North Atlantic subpolar gyre: a comparison of estimates derived from new gravity and oceanographic measurements*. J. Geophys. Res. Oceans 116.

Hirschi, J., Baehr, J., Marotzke, J., Stark, J., Cunningham, S., & Beismann, J. O., 2003. *A monitoring design for the Atlantic meridional overturning circulation*. Geophysical Research Letters, 30(7).

Holliday, N. P., and Coauthors, 2008: *Reversal of the 1960s to 1990s freshening trend in the northeast North Atlantic and Nordic Seas*. Geophys. Res. Lett., 35, L03614.

Johnson, G. C., and N. Gruber, 2007. *Decadal water mass variations along 20°W in the northeastern Atlantic Ocean.* Prog. Oceanogr., 73, 277–295.

Jungclaus J.H., Haak H., Latif M., Mikolajewicz U., 2005. *Arctic-North Atlantic interactions and multidecadal variability of the meridional overturning circulation*. J Clim 18:4013–4031

Jungclaus J. H., Lohmann K., Zanchettin D., 2014. *Enhanced 20th century heat transfer to the Arctic simulated in context of climate variations over last millennium*. Clim. Past. 10, 2201–2213.

Kantha H. L., and Clayson A. C., 2000. Numerical Models of Oceans and Oceanic Processes. pp 2-3

Katsman, C., Spall, M., Pickart, R., 2004. *Boundary current eddies and their role in the restratification of the Labrador Sea.* J. Phys. Oceanogr. 34 (9), 1967–1983.

Levermann, A., & Born, A., 2007. *Bistability of the Atlantic subpolar gyre in a coarse-resolution climate model*. Geophysical Research Letters, 34(24).

Lohmann K., Helge D., and Mats B., 2009. *A possible mechanism for the strong weakening of the North Atlantic subpolar gyre in the mid-1990s.* Geophysical Research Letters 36, 15

Maier-Reimer, E., 1993. *Geochemical cycles in an ocean general circulation model: Preindurstrial tracer distributions*. Global Biogeochem. Cycles, 7, 645–677.

Maier-Reimer, E., Kriest I., Segschneider J., and Wetzel P., 2005. Technical description of the HAMburg Ocean Carbon Cycle model, version 5.1 (HAMOCC5.1), and of its interface to MPIOM. Reports on Earth System Science, Max Planck Institute for Meteorol., Hamburg. [Available at http://edoc.mpg.de/get.epl?fid517575&did5249293&ver50.]

Majewski, D., 1991. *The Europa modell of the Deutscher Wetterdienst*. Seminar Proceedings ECMWF, vol. 2, pp. 147–191, ECMWF, Reading, U. K.

Mamayev, O. I., 2010. Temperature-salinity analysis of world ocean waters (Vol. 11). Elsevier.

Manabe, S., & Stouffer, R. J., 1999. *The role of thermohaline circulation in climate*. Tellus B, 51(1), 91-109.

Marzocchi, A., Hirschi J. J.-M., Holliday N. P., Cunningham S. A., Blaker A. T., Coward A. C., 2014. *The North Atlantic subpolar circulation in an eddy-resolving global ocean model*. J. of Marine Systems 142, 126–143.

Medhaug, I., Langehaug, H.R., Eldevik, T. *et al*., 2012. *Mechanisms for decadal scale variability in a simulated Atlantic meridional overturning circulation***.** Clim. Dyn. 39: 77.

Moreno-Chamarro E., Zanchettin D., Lohmann K., Jungclaus J. H., 2015. *Internally generated decadal cold events in the northern North Atlantic and their possible implications for the demise of the Norse settlements in Greenland*. Geophys. Res. Lett., 42.

Moreno-Chamarro, E., Zanchettin D., Lohmann, K., Jungclaus J. H., 2016. *An abrupt weakening of the subpolar gyre as trigger of Little Ice Ag -type episods.* Clim. Dyn. (2017) 48 (3-4), 727.

Pohlmann H., Botzet M., Latif M., Wild M., Tschuck P., 2004. *Estimating the long-term predictability potential of a coupled AOGCM*. J Clim 17:4463–4472.

Rahmstorf, S., 2003. *Thermohaline circulation: The current climate*. Nature, 421(6924), 699.

Rhein, M., Kieke, D., Huettl-Kabus, S., Rossler, A., Mertens, C., Meissner, R., Klein, B., Böning, C.W., Yashayaev, I., 2011. *Deep water formation, the subpolar gyre, and the meridional overturning circulation in the subpolar North Atlantic*. Deep-Sea Res. II Top. Stud. Oceanogr. 58 (17–18), 1819–1832.

Robson, J. I., Sutton, R. T., & Smith, D. M., 2012. *Initialized decadal predictions of the rapid warming of the North Atlantic Ocean in the mid 1990s*. Geophysical Research Letters, 39(19)

Sein, D. V., Mikolajewicz U., Gröger M., Fast I., Cabos W., Pinto J. G., Hagemann S., Semmler T., Izquierdo A., Jacob D., 2015. *Regionally coupled atmosphere-ocean-sea ice- marine biogeochemistry model ROM: 1. Description and validation*. J. Adv. Model. Earth Syst., 7, 268–304.

Smith, R.D., M.E. Maltrud, F.O. Bryan, and M.W. Hecht, 2000: *Numerical Simulation of the North Atlantic Ocean at 1/10°*. J. Phys. Oceanogr., 30, 1532–1561.

Smith, R. S., and J. M. Gregory, 2009. *A study of the sensitivity of ocean overturning circulation and climate to freshwater input in different regions of the North Atlantic*, Geophys. Res. Lett., 36, L15701.

Stössel, A., 1992. *The Hamburg sea-ice model*. Tech. Rep. 3, Ger. Clim. Comput. Cent., Hamburg, Germany.

Talley L. D., Pickard G. L., Emery W. J. and Swift J. H., 2001. Descriptive Physical Oceanography: An Introduction. pp 43

Taylor, K. E., Stouffer R. J., Meehl G. A., 2012. *An overview of CMIP5 and the experiment design*. Bull. Am. Meteorol. Soc., 93, 485–498.

Treguier, A.M., S. Theetten, E.P. Chassignet, T. Penduff, R. Smith, L. Talley, J.O. Beismann, and C. Böning, 2005: *The North Atlantic Subpolar Gyre in Four High-Resolution Models*. J. Phys. Oceanogr., 35, 757–774.

Yashayaev, I., 2007. Hydrographic changes in the Labrador Sea, 1960–2005. Prog. Oceanogr. 73 (3–4), 242–276.

Yoshimori M., Raible C. C., Stocker T. F., Renold M., 2010. *Simulated decadal oscillations of the Atlantic meridional overturning circulation in a cold climate state*. Clim. Dyn. 34(1), 101–121.

Zanchettin D., Gaetan C., Arisido M. W., Modali K., T. Toniazzo, N. Keenlyside, Rubino A., 2017. *Structural decomposition of decadal climate prediction errors: A Bayesian approach.* Sc. Rep. 7, 12862.

APPENDIX: R codes

In the following, a list of codes used to perform the statistical analyses with the software R within the four transient simulations *NA* and *GI3*.

```
#### TIME SERIES ANALYSIS

## time series creation

file.nc <- open.nc("filename.nc")
variable.v <- var.get.nc(ncfile = file.nc, variable = "varID", start = c(1,1,1))

time.v <-  convertDateNcdf2R(spg_arn, origin = as.POSIXct("1920-01-31 00:00:00", tz = "UTC"),
time.format ="%Y-%m-%d %H:%M:%S")

variable_ts <- ts(variable.v, start = c(YYYY,MM), end = c(YYYY,MM), frequency = 12)
plot(variable_ts, ylab=" ", xlab="Time(Years)")


## Loess decomposition and Kernel smoothing

tt <- time(variable_ts)
variable_stl<- stl(variable_ts, s.window="periodic")
plot(spg_stl$time.series)
variable_trend<-(variable_stl$time.series[,2])
variable_smooth<-ksmooth(tt,variable_ts)

## Annual anomalies

variable_annual <- aggregate(variable_ts, nfrequency=1, FUN=mean)
variable_anomaly <- variable_annual - mean(variable_annual)


#### REGRESSION AND CORRELATION ANALYSIS

## desonalized the time series creation

myf<-function(y,s.window="periodic")

{
  if (sum(is.na(y))> 0) {
    return(rep(NA,length(y)))
  }
  y.ts<-ts(y, start = 1920, end = 2006, frequency = 12)
  f<-stl(y.ts,s.window = s.window)
  variable<-apply(f$time.series[,2:3],1,sum)
  return(variable)
}

variable.ts <- apply(variable.v,c(1,2),myf)

## kernel smoothing of the gridded time series
```

```
ts<-apply(variable.ts, c(1,2), function(x)  ts(unlist(x[])))
kernel<-apply(ts, c(1,2), function(x) ksmooth(t, (unlist(x))))
variable.k<-matrix(lapply(kernel, function(x) ({x[c("y")]})), nrow=nrow(variable.v),
ncol=ncol(variable.v)


### lead – lag correlation analysis

a<-variable.k

k<-  # k: -36:12:36 & K:-8:2:8

cor<-matrix(NA,nrow(a),ncol(a))
zz<-unlist(list(spg.v))[1:t]

if (k == 0) {
  x <- zz
} else if (k < 0) {
  x <- zz[1:(t-abs(k))]
} else {
  x <- zz[(k+1):t]
}

for (i in 1:nrow(a)) {
  for (j in 1:ncol(a)){
    if (k == 0) {
      y <- unlist(a[i,j])[1:t]
    } else if (k < 0) {
      y <- unlist(a[i,j])[(abs(k)+1):t]
    } else {
      y <- unlist(a[i,j])[1:(t-k)]
    }
    if (sum(is.na(y)) < length(x)){
    out<-cor.test(x,y)
    corr[i,j]<-out$estimate
    corrp[i,j]<-out$p.value
    if (corrp[i,j] > 0.05) {
      corr[i,j]<-NA    }
  }
}

lat<-var.get.nc(file.nc, "lat", start = c(1,1))
lon<-var.get.nc(file.nc,"lon", start = c(1,1))

image.plot(corr, main ="", zlim=c())
plot(wrld_simpl,add=TRUE)


## lead - lag regression analysis

k<- # k: -36:12:36 & k:-8:2:8
reg<-matrix(NA,nrow(a),ncol(a))
```

```
regp<-matrix(NA,nrow(a),ncol(a))
zz<-unlist(list(spg.v))[1:t]

if (k == 0) {
  x <- zz
} else if (k < 0) {
  x <- zz[1:(t-abs(k))]
} else {
  x <- zz[(k+1):t]
}

for (i in 1:nrow(a)) {
  for (j in 1:ncol(a)){
    if (k == 0) {
      y <- unlist(a[i,j])[1:t]
    } else if (k < 0) {
      y <- unlist(a[i,j])[(abs(k)+1):t]
    } else {
      y <- unlist(a[i,j])[1:(t-k)]
    }
    if (sum(is.na(y)) < length(x)){
      out<-summary(lm(y~x))
      reg[i,j]<-out$coefficients[2,1]
      regp[i,j]<-out$coefficients[2,4]
    }
  }
}

### WAVELET ANALYSIS

x1<- spg_anomaly
y1<-  variable_anomaly

df<-data.frame(x1,y1)
my.w<-analyze.coherency(df, my.pair = c(1,2), make.pval = TRUE)

wc.image(my.w, color.key = "quantile", n.levels = 100, siglvl.arrow = 0.05,
        legend.params = list(lab = "wavelet power levels"),
        periodlab = "period (months)",
        label.time.axis = TRUE)

wc.image(my.w, color.key = "interval", n.levels = 100, siglvl.arrow = 0.05,
        legend.params = list(lab = "wavelet power levels"),
        periodlab = "period (months)",
        label.time.axis = TRUE)

wc.phasediff.image(my.w, which.contour = "wc", n.levels = 100, label.time.axis = TRUE, timelab
= "time")
```